Electrical Resistivity Imaging of Preferential Flow through Surface Mine Valley Fills with Comparison to Other Land Forms

Breeyn M. Greer

Thesis submitted to the faculty of the Virginia Polytechnic Institute and State University in partial fulfillment of the requirements for the degree of

Master of Science
In
Civil Engineering

Erich T. Hester, Chair
Thomas J. Burbey
Carl E. Zipper

March 27, 2015
Blacksburg, VA

Keywords: Electrical resistivity imaging, surface coal mine, mountaintop removal mining, preferential flow, specific conductance, artificial rainfall

Electrical Resistivity Imaging of Preferential Flow through Surface Mine Valley Fills with Comparison to Other Land Forms

Breeyn M. Greer

Surface coal mining has caused significant land-use change in central Appalachia in the past few decades. This landscape altering process has been shown to degrade water quality and impact aquatic communities in the mining-influenced headwater streams of this biodiverse ecoregion. Among pollutants of concern is total dissolved solids (TDS) which is usually measured via its surrogate parameter, specific conductance (SC). The SC of valley fill effluent is a function of fill construction methods, materials, and age; yet hydrologic studies that relate these variables to water quality are sparse due to the difficulty of implementing traditional hydrologic measurements in fill material. We tested the effectiveness of electrical resistivity imaging (ERI) to monitor subsurface hydrologic flow paths in valley fills. ERI is a non-invasive geophysical inverse technique that maps spatiotemporal changes in resistivity of the subsurface. When a resistance or conductive change is induced in the system, ERI can reveal both geologic structure and hydrologic flows. We paired ERI with artificial rainfall experiments to track highly conductive infiltrated water as it moved through the valley fill. The subsurface structure of two other landforms were also imaged to confirm variations between forms. Results indicate that ERI can be used to identify the subsurface geologic structure as well as track the advancing wetting front and preferential flow paths. We observed that the upper portion of a fill develops a profile that more closely resembles soil with smaller particle sizes, while the deeper profile has higher heterogeneity, with large rocks and void spaces. The sprinkling experiments revealed that water tends to pond on the surface of compacted areas until it reaches preferential flowpaths, where it infiltrates quickly and migrates deeply or laterally. We observed water moving from the surface down to a 20 meters depth in one hour and 15 minutes, and to a depth of 10 meters in just 45 minutes. We also observed lateral preferential flow downslope within 5 meters of the surface, likely due to transmissive zones between compacted layers along the angle-of-repose. Finally, when compared to other landscapes we were able to see that a filled highwall slope has larger rocks near the surface than the valley fill, but a similar degree of heterogeneity throughout; while the natural slope has less heterogeneity at depth as is expected in consolidated bedrock. ERI applications can improve understanding of how various fill construction techniques influence subsurface water movement, and in turn aid in the development of valley fill construction methods that will reduce environmental impacts.

Acknowledgments

I would like to thank Wells Fargo and Company for funding this study through the Clean Technology and Innovation Grant (views expressed in this document are those of the authors, and not necessarily those of Wells Fargo). I would like to thank the Powell River Project for their assistance and cooperation. I would like to thank all of the field assistants I had throughout the project including: Elyse Clark, S.M. Masud Rana, Abenezer Nida, Emily Baer, Chris Driscoll, and Ian Goodwin. I would like to thank my family, The Greers as well as Amanda Schick for all of their encouragement over the past two years. Lastly I would like to thank my advisor Erich Hester for providing me both guidance and creative freedom and my committee members Thomas J. Burbey and Carl Zipper for their knowledge and support through the duration of this project.

Table of Contents

List of Figures

List of Tables

Chapter 1 – Introduction and Literature Review

1.1 Mountaintop Removal Mining and Valley Fills

The technological advancements that have been made in the last century have revolutionized every industry, and the coal mining industry is no exception. An increased demand for energy, combined with larger and more powerful earth moving equipment has resulted in Mountain Top Removal Mining (MTM) for coal (Lindberg et al., 2011) also known as surface coal mining. This form of mining involves overburden and coal removal for depths up to 300 meters (Peng, 2000), and results in the local topography and land cover being drastically changed. Mined areas are often returned to their approximate original contour (AOC), yet excess fill is left over due to the expanded volume of rock once it is broken apart during mining. Part of the reclamation process is therefore the construction of valley fills (VF), in which this excess overburden is placed in adjacent valleys, covering headwater streams (Figure 1-1). Reclamation also includes a sediment pond downstream of the VF which typically remains in place for several years before removal. MTRM/VF operations result in changes to both the hydrology and water quality of the area that persist for decades after reclamation has been completed (Evans et al., 2014; Miller and Zegre 2014). This section documents these environmental changes by utilizing previously published literature.

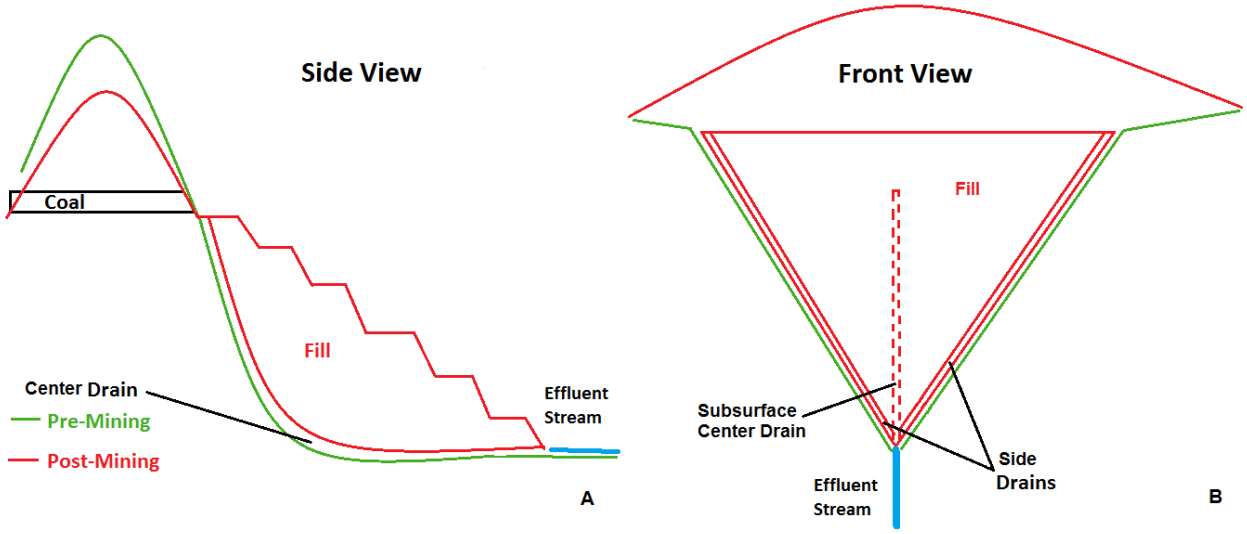

Figure 1-1. Side and Front View of a Valley Fill. Shown is how the valley fill alters the original landscape. Panel A shows the side view, while panel B shows the front view. The drains act as preferential flow paths for stormwater which emerges as an effluent stream at the bottom.

In the United States, MTRM coal mining is primarily confined to the Appalachian Coalfield Region (ACR) consisting of eastern Kentucky, southern West Virginia, northeastern Tennessee, and southwest Virginia (Lindberg et al., 2011). Because it escaped glaciation during the last ice age, this region is one of the oldest mountainous ecoregions in the world (Bernhardt and Palmer, 2011). Due to its age, climate, and topography, this region has very high species richness (Bernhardt and Palmer, 2011). The ACR is home to many headwater streams, 4,000 km of which have been buried by valley fills as of 2012 (EPA, 2011). MTRM alters water quality

downstream with potential to impact ecosystems (Johnson, 2010). Over 600,000 hectares have been mined in the ACR (Zipper et al., 2011) and MTRM/VF is now the largest land use change in the region (Sayler, 2008). There are some law and regulations in place, such as those implementing Surface Mining Control and Reclamation Act (SMCRA) which declared that during reclamation landscapes must be returned to their approximate original contour (AOC) (US Congress, 1977). The Clean Water Act (CWA) allows MTRM to occur, but also requires that National Pollution Discharge Elimination System (NPDES) permits for mine effluent as well as all mine related stormwater until it meets water quality criteria (EPA, 2011). However the effectiveness and enforcement of these often narrative (non-numeric) requirements is undetermined (EPA, 2011; Bernhardt and Palmer, 2011); for example, total dissolved solids limitations are typically not stated in such permits. The Clean Water Act also requires a Section 404 permit for filling of streams which is required before building valley fills. MTRM mining and VFs result in hydrologic, water quality, and biological effects that are long lasting; each of which is addressed below.

1.1.1 Hydrologic Effects

MTRM/VF results in many hydrologic changes that persist decades after the reclamation phase is completed (Evans et al., 2014; Miller and Zegre, 2014). These hydrologic changes in turn affect water quality via drastically increasing weathering by-product release as water moves through the fill (discussed below). There are at least three main hydrologic effects of MTRM / VF operations: changes to the stormwater runoff hydrograph, increase in volume and duration of baseflow, and the formation of unnatural flow paths over and through the mined landscape. These three fundamental hydrologic changes may result in increased flooding downstream (Phillips, 2004; Ferrari, 2009). While there have been a number of hydrologic studies, the cumulative effects of these hydrologic changes is poorly understood (Miller and Zegre, 2014). Confounding traditional hydrologic techniques such as groundwater wells or infiltrometers are structural changes to the catchment caused by overburden removal and replacement, such as those to watershed boundaries, landscape slope, and cover. The rocky and porous nature of mine spoil adds additional challenges.

Changes to the storm runoff hydrograph are primarily the result of surface compaction and alteration of the subsurface structure (Daniels and Zipper, 1997; Holl, 2002). Compaction results in decreased infiltration and evapotranspiration via inhibiting forest re-growth (Daniels and Zipper, 1997) which in turn increases overland flow (Guebert and Gardner, 2001). In some cases a thin layer of top soil is replaced over the spoil, however this soil does not retain the pre-mining soil structure and only accounts for at most 10% of total fill depth (Guebert and Gardner, 2001). Guebert & Gardner (2001) found that infiltration rates on soil-covered mine spoil tend to increase with time without decreasing runoff rates due to increased throughflow via macropores. The subsurface of a valley fill is composed of crushed rock of various sizes with a variety of pore sizes rather than a fairly uniform soil matrix; which results in more variable hydraulic conductivity than a natural subsurface (Hawkins, 2004). Constructed into valley fills is usually a series of drains, which are simply areas of large boulders that act as preferential flow paths. Preferential flow paths have also been documented in the fill at large (ex. Wunsh, 1999; Hawkins and Aljoe, 2007).

Changes to the storm runoff hydrograph manifest in three ways: decreased time to peak, increased peak flow rate, and increased tailing (Guebert and Gardner, 2001; Messinger, 2003; Negley and Eshleman, 2006; McCormick et al., 2009). In summation, this shift can be conceptualized as a transition from saturation excess overland flow to infiltration excess overland flow. Many studies have also concluded than MTRM/VF activities result in larger total stormflow volumes (Wiley and Brogan, 2003 Messinger, 2003, Messinger and Paybins, 2003). Messinger (2003) noted that during all storms with rainfall intensity > 0.75 in/hour, a mined tributary had larger flow volumes than an unmined tributary. However, the reverse was true during smaller storms. This study also noted that the mined tributary had the expected alteration of increased peak flow rate, but surprisingly has increased tailing of the hydrograph. Similar tailing was not seen in the unmined tributary. Conversely, in another case, peak flow rates were higher in mined catchments yet total flow volume was less due to loss to subsurface mine tunnels (McCormick et al., 2009), this finding is less common, but not original (Puente and Akins, 1989). Overall, MTR/VF operations typically result in flashier hydrographs and increased total flow volumes (Miller and Zegre 2014), which together increase downstream risk of flooding.

Increased risk of flooding as a result of MTR/VF activities poses a danger to communities downstream which has been well documented in the last decade. Hydrologic response to storm events is more variable in mined catchments than in forested catchments (Wiley and Brogan, 2003). Phillips (2004) corroborated this finding and further concluded that MTRM/VF activities tend to increase the flood risk. A positive linear relationship was found between mined watershed percentage and the peak flow rate for a given storm using a location based calibrated model (Figure 1-3) (Ferrari et al., 2009). This modeling study also concluded that in regards to flooding, the mining and reclamation process looks more like urbanization than deforestation in that mining tends to primarily increase the magnitude of small, frequent floods rather than large infrequent floods. These studies demonstrate the high degree of sustained disturbance that occurs at MTRM/VF sites and the flood risk that accompanies it.

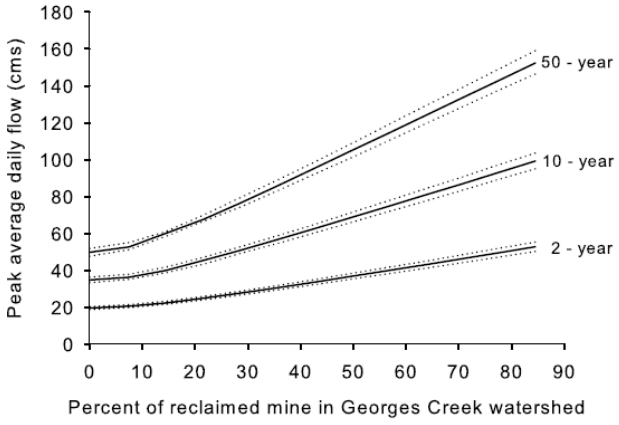

Figure 1-2. Peak Flow Rates for various Storms (Ferrari et al., 2009). This graph relates the linear relationship between the percentage of up-watershed mined land and peak flood flow rates for storms of various recurrence intervals. The graph is based on hydrograph simulation modeling.

Changes to baseflow, in both quantity and variability have also been documented at MTRM/VF sites. Multiple studies have found that the volume of baseflow is increased at outlet streams of valley fills (Green, 2000; Wiley et al., 2001; Messinger and Paybins, 2003, Zegre et al., 2014). This is likely due to both a steady discharge of groundwater and increased stormflow tailing from both the upland spoil piles and the adjacent VF (Dickens, 1985; Miller and Zegre, 2014). Studies have shown that an upland spoil pile will reach steady state when 20% of its thickness is saturated with groundwater (Hawkins, 2004). Saturated pore space combined with minimal slope of bedrock beneath removed coal layer and subsequently replaced spoil encourages slow, steady discharge from the upland areas, with quicker discharge through the slanted valley fills (Wunsch, 1999). This phenomenon is also known as transient storage (Zegre et al., 2014). Increase in baseflow due to discharging groundwater and transient storage is most dramatic during dry periods, affecting natural seasonal flow variations which impact local ecosystems (Messinger and Paybins, 2003, Zegre et al., 2014).

The final way in which the mining and reclamation process affects hydrology is that valley fills result in both surface water and groundwater flowing along unnatural flow paths. Because both spoil piles and valley fills are composed of compacted crushed rock overlain on large boulders, the natural infiltration, throughflow, and return-flow processes are disrupted. Water either does not infiltrate at all, infiltrates through the mine soil matrix, or infiltrates quickly along preferential flow paths (previously referred to as pseudokarst, Caruccio and Geidel 1984) (Wunsh et al., 1999; Miller and Zegre, 2014). These preferential flow paths have previously been used as an explanation for complex data, although these flowpaths have not been observed directly. Matrix flow and preferential flow components have been assumed to be disconnected (Hawkins and Aljoe, 2007), meaning that water may not have a clear path from one region of the fill to another. The points along the surface and in the subsurface at which water changes directions or routes have been referred to as control points (Evans et al., in press) This pseudokarst hydrologic regime has recently been expanded upon (Miller and Zegre, 2014; Evans et al. In Press), however the relationship between structure, hydrology, and water quality remains unknown.

1.1.2 Water Quality Effects

In addition to hydrologic changes as a result of MTRM/VF, there are also relevant changes to water quality. The changes to water quality that are most drastic include: increased total dissolved solids (TDS), increased pH, and high concentrations of heavy metals. These water quality changes in turn impact biodiversity in the region. Valley fills are at the heart of this issue as it has been shown that valley fills have a stronger correlation with downstream water quality degradation than the actual surface mine (Cormier et al., 2013). Increased TDS is the most important and will be discussed first.

Elevated TDS has been shown to be a significant impact of MTRM/VF on headwater stream water quality (Griffith et al., 2012). Elevated TDS acts as a stressor to aquatic biology by inducing an osmotic pressure on small organisms (Pond et al., 2008; Bernhardt and Palmer, 2011). High TDS is the result of large quantities of broken rock undergoing accelerated weathering via exposure to water and air. TDS is often measured through its surrogate, specific

conductance (SC), because it can be measured instantaneously in the field. SC is generated by the presence of dissolved ions in solution; defined as the product of the concentration of each ion, the absolute value of its charge, and the ion-specific equivalent conductance (Griffith et al., 2012). The relationship between SC and concentration of SO_4^{2-}, Ca^{2+}, Mg^{2+}, Se, HCO_3, and total dissolved nitrogen (TDN) is strong, but will vary dependent on fill properties such as age and construction material (example, Figure 1-4) (Lindberg et al., 2011; Parker, 2013). SC has been shown to increase with increasing area of active mining, valley fill, and total mining in the watershed. However, a study by Cormier et al. (2013) found SC is most strongly linked with valley fill area. Primary anion contributors to SC in MTRM/VF impacted streams are usually SO_4^{2-} and HCO_3, derived primarily from weathering rock (Cormier et al., 2013; Parker, 2013). Since high SC is a result of weathering, the concentrations stay high even after multiple decades of reclamation (Merricks et al., 2007, Evans et al., 2014). The natural background SC for mountainous headwater streams in this area is 10 – 300 µS/cm but the range for MTRM affected streams is a central West Virginia watershed was found to be 1000 – 2500 µS/cm (Lindberg et al., 2011). The EPA has recently determined that SC levels of greater than 300 µS/cm is harmful to aquatic life (US EPA, 2010).

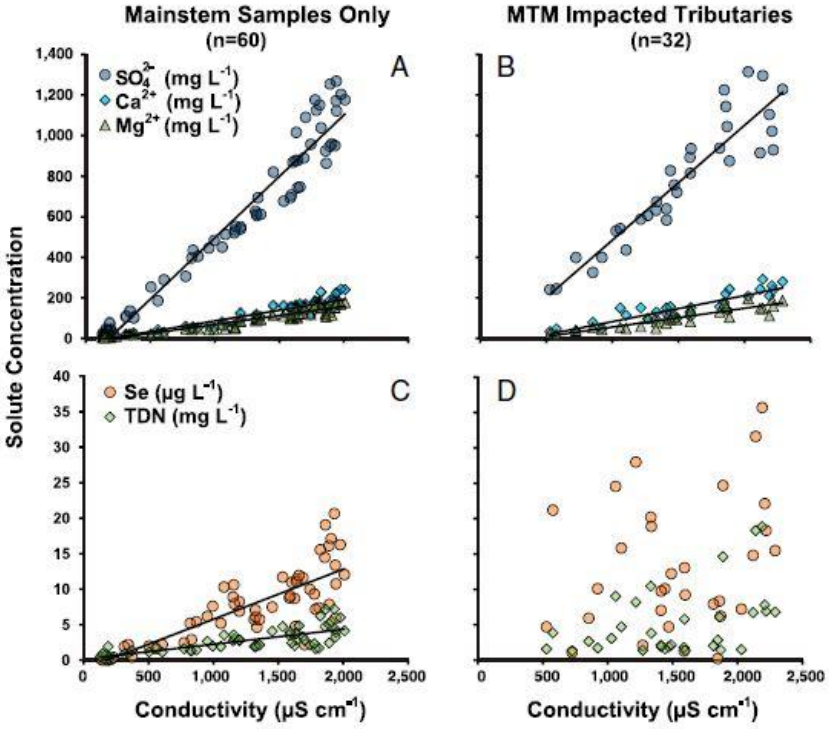

Figure 1-3. Solute Concentrations vs. Conductivity (Lindberg et al., 2011). These graphs demonstrate that conductivity (SC) is a good predictor of sulfate, calcium, magnesium, and to a lesser degree selenium and total dissolved nitrogen in the watershed studied.

Taking a longitudinal stream network approach, EC, pH, and water temperature increase as mine-impacted tributaries joined Buckhorn Creek, in Kentucky (Figure 1-5) (Johnson, 2010). The only feasible way to reduce SC once elevated through dilution. The size and number of

tributaries to Buckhorn Creek also show that increases in SC can be far-reaching. Shifting to a temporal perspective, Kirk and Maggard (2004) measured SC twice annually from 1995 to 2003, during which a surface mine was developed upstream. They noticed a 300 us/cm increase in the spring and a 1,400 us/cm increase in autumn measurements from 1996 to 2003. Seasonality of SC in streams has not been thoroughly documented, however is has been observed that measurements taken in the summer consistently had high SC values in congruence with times of low flow (Green et al, 2000). Higher SC in baseflow results from baseflow having the largest retention time in the fill and subsequently collecting the most salts. On a larger temporal sale, Evans et al. (2014) found SC in valley fill effluent to be highest, on average, at 10 years after the start of VF construction, after which it begins to decline.

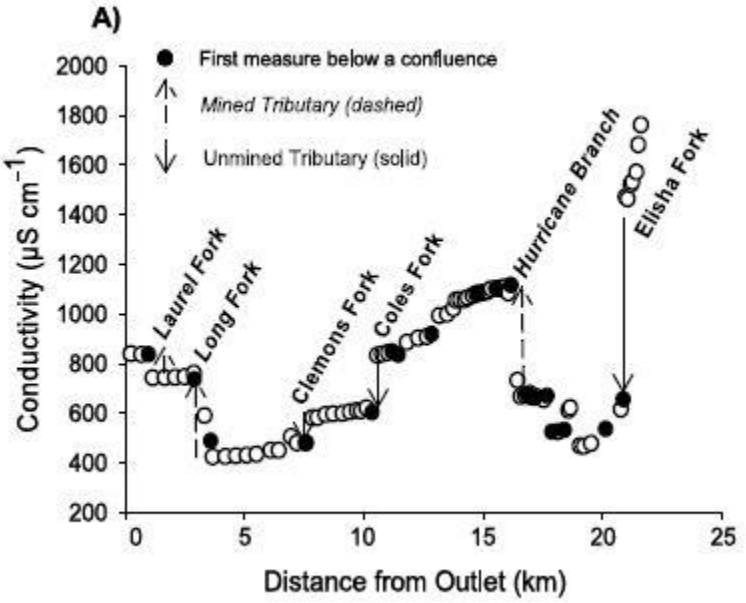

Figure 1-4. Influence of Mined and Unmined Tributaries on Conductivity (Johnson, 2010). Streamflow is from right to left.

Alkaline, or high-pH, valley fil effluent is common in many streams affected by MTRM (Bernhardt et al, 2011; Lindberg et al., 2011). Less is known about the effects of increased pH in Appalachian coalfield streams than is known about effects of acidity, which has been more thoroughly studied. There have been a few studies on the cause of this phenomenon, all of which conclude that it is the result of weathering sedimentary rocks that contain carbonates (Hartman et al., 2005; Pond et al., 2008; Palmer et al. 2010). The weathering of Appalachian mine spoil rocks results in pyrite (FeS2) being oxidized to form sulfate (SO_4^{2-}) (Griffith et al., 2012). Pyrite oxidation accelerates weathering of carbonate minerals that are also present in many of these rocks, resulting in valley fill effluents with high Mg^{2+}, Ca^{2+}, HCO_3^-, SO_4^{2-}, and thus high pH (Palmer et al. 2010; Bernhardt and Palmer, 2011, Lindberg et al., 2011). Because this high pH is caused by weathering, it continues and even intensifies years after reclamation has been completed as the primary TDS ion shifts from SO_4^{2-} to HCO_3^- with time.

Heavy metals and other trace elements are also present in valley fill streams. These include Mn, Fe, and Al and are primarily released during active mining and the early phases of reclamation (Ferrari, 2009, Messinger 2003). This implies that the metals are flushed out of the system quickly and are not a weathering byproduct. One finding to support this is that there was no significant relationship found between metal concentrations and weathering byproduct concentrations (Lindberg et al., 2011). Some trace elements bioaccumulate in aquatic organisms which intensifies their toxicity in animals higher up in the food chain and increases their residence time in the ecosystem. Another element of particular concern in mine spoil effluent is selenium (Se). Se is very toxic to fish and birds when bioaccumulated and is soluble in alkaline waters (Lindberg et al., 2011). High Se concentrations result in both reproductive failure and physical deformities in fish (Paybins et al., 2000, Palmer et al., 2010). Se pollution from mining is of great concern in the Appalachian coalfields.

1.1.3 Species Richness Effects

One well known measure of ecosystem health is species richness, which refers to the number of species present in an ecosystem. Species richness is a good indicator of overall stream health because it measures how organisms handle the various types of pollution, rather than measuring specific solutes and trying to correlate them to toxicity. Richness of benthic macroinvertebrate species is used as a water quality metric by state agencies in both VA and WV (Pond, 2010). Due to the described water quality issues many streams in the ACR have experienced a loss of certain macroinvertebrate species. Pond et al., (2008) showed that there is a direct relationship between the extent of up-watershed mining and a loss of Ephemeroptera (mayfly) species richness and relative abundance. This study also compiled evidence that mining impairs stream biology by shifting species assemblages, loss of mayflies, which are an indicator of overall stream health, and changes in individual species metrics. In a follow-up study, species richness was used to relate numeric water quality measurements with ecological disturbance of various land-uses across central Appalachia (Pond, 2010). SC and pH were found to be significantly higher at mine-impacted sites; these sites also had a significantly lower quantity of mayflies and mayfly taxa richness. Mayfly relative abundance was found to correlate most strongly with EC, with a threshold-like response of mayfly loss when SC was higher than 175 uS/cm, which is much lower than the EPA's recommendation of 300 uS/cm.

Water quality parameters and benthic macroinvertebrate community differences between natural and valley fill-impacted streams was studied by Hartman et al. (2005). Benthic macroinvertebrate community structure was measured via the rapid bioassessment protocol (RBP) (US EPA, 1999). SC had a statistically significant increase in valley filled streams. The RBP results showed a significant difference for six individual species between the natural and valley fill impacted streams; however, there was not a significant difference in overall aquatic organism densities, possibly due to sampling during a time of low bio-productivity.

1.2 Electrical Resistivity Imaging

1.2.1 Introduction and Operation

Electrical Resistivity Imaging (ERI) is a non-invasive subsurface imaging technique that may be used to spatiotemporally record changes in material or fluid through change in the material or

fluid property of resistivity. Electrical resistivity is the ability of a fluid or material to resist electrical current and is defined as the inverse of electrical conductivity (Herman, 2001). This is useful for a variety of geological applications such as investigation of the water table, fault lines, or pipe leaks. In this context, it is used to distinguish between rock and water. This section discusses ERI theory, data analysis, and relevant hydrologic applications. The ERI process consists of two main parts: the survey and data analysis via inversion. ERI is limited by the cost of the equipment, the spatial-temporal resolution relationship, and the accuracy of the analytical inversion process (all discussed below).

Prior to conducting an ERI survey, background data is collected. This must be done in advance because basic information on physical and hydrologic site parameters are necessary for data collection and analysis. A topographic survey is needed to pair with the ERI survey. The size of the site is relevant when designing the ERI survey. The transect length (linear length of land surface in which the electrodes are placed and the subsurface mapped), depth, and approximate spatial resolution desired must be pre-determined. There is an integral relationship between the transect length and imaging depth; in general, accuracy is greatly diminished below depths greater than one fifth of the total transect length (Roningen and Burbey, 2012). It is also useful to take note of relevant surface geologic features, for example electrodes cannot be installed into bedrock so the site must have some sort of granular or soil cover at least as deep as the electrodes are long (45 cm).

The ERI survey is conducted with an earth resistivity meter (earth meter) which interprets a user-generated command file. The command file contains the spatial coordinates of where the electrodes will be installed, the array, and the sequence for the survey (terms are defined below; AGI, 2009). The earth meter collects data sets known as surveys which consist of hundreds of measurements. Each measurement is taken with four electrodes (i.e. quadripole) consisting of a current (I) pair and a potential difference (V) pair (Ward et al., 2010). The order of electrodes within the quadripole is called the array (AGI, 2009). There are many arrays available, but for this application of 2D earth resistivity, dipole-dipole is most common due to its sensitivity to vertical heterogeneity and accuracy at depth (Herman, 2001; Seaton and Burbey, 2002; Dahlin and Zhou, 2004). A dipole-dipole array is set up such that current (I) is injected between two contiguous electrodes, and then voltage (V) is read between two separate contiguous electrodes (Figure 1-6, represented by I_1 I_2 and V_1 V_2 within each quadripole) (Herman, 2001). Alternatively, for example in a Werner array V is measured between two electrodes that are nested within the two that inject I (Herman, 2001). While the array is the quadripole order for a single measurement, the command file also contains the sequence of measurements for the entire survey (Figure 1-6). The sequence specifies that the earth meter starts each successive quadripole at intervals of one electrode (Quadripole 1, n=1), moving up the transect one electrode at a time. The data level (n) indicates both the n^{th} pass along the transect and the depth into the subsurface. Passes along the transect are repeated, skipping one more electrode each time (Quadripole 18 (n=2) and Quadripole 32 (n=3)) and collecting fewer measurements each time until the final pass contains only one measurement with I_1 and V_2 being at either end of the transect (Quadripole 56, n=6). The result of all of the measurements is a collection of measurements which make up the survey and are used to produce an image, known as a tomogram.

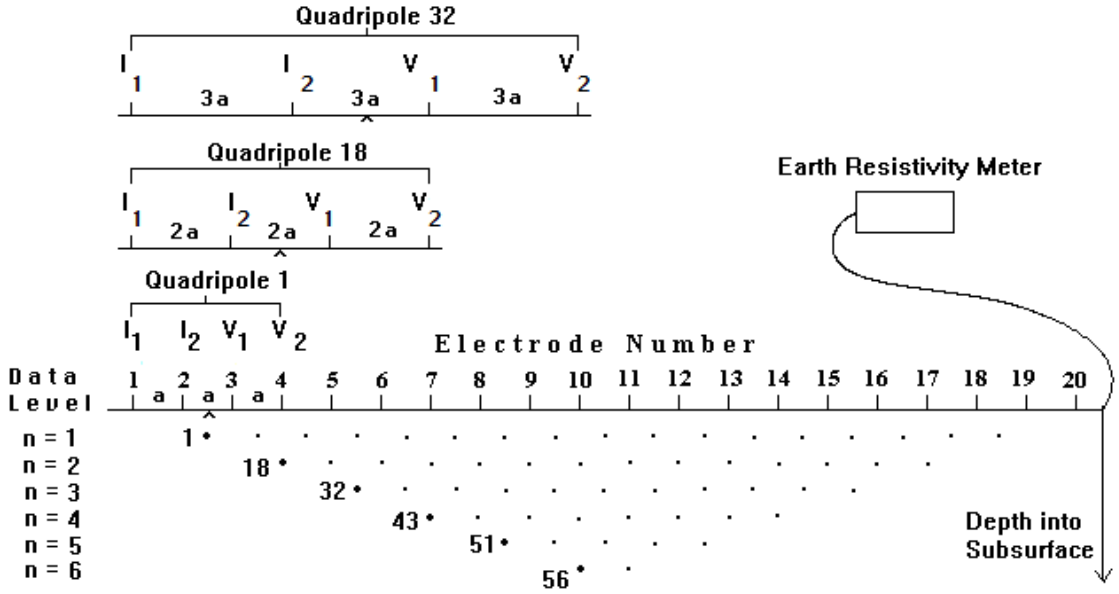

Figure 1-5. Sequence of Readings (adapted from Geotomo, 2013). The orientation of electrodes in dipole-dipole array is displayed by I_1, I_2, V_1, and V_2. An example of the sequence is displayed with quadripoles 1, 18, and 32. This is done in horizontal layers increasing in depth into the subsurface (n=1-6) with increasing depth and electrode spacing at each layer.

The ERI data collection process is automated and completed once the electrodes comprising the transect are installed in the ground. First, the electrodes are hammered in at the pre-determined spatial intervals. The accuracy of the survey is somewhat dependent on how precisely these electrodes are placed, however there are instances where a rock or tree root will make installation impossible in which slight displacement may be required. The accuracy of the survey is heavily dependent on the electrode – earth connection. This is ensured by wetting the soil so that it expands around the electrode and via the resistance test, explained later. Second, the electrode cables are reeled out and the electrodes are connected. The cables have address numbers associated with each electrode.

Third, all of the cables are attached appropriately: the battery to the control box, the electrode cables to the switchbox, the switchbox to the control box via a connecting cable. A simplified diagram for the Advanced Geosciences Inc. (AGI) Supersting R8 (Austin, TX) is shown in Figure 1-7. Fourth, the earth meter completes a resistivity test to ensure good electrode-earth connection. The resistance test is completed automatically and entails injecting current and reading voltage between contiguous electrodes all the way up the transect. Outlying resistance values (relative to the majority of the transect) serve as an indication of an electrode being installed on top of a rock or into a void space. The electrodes with poor connection are then reinstalled and the resistance test run again, until there are no outliers. Fifth, a new data file is created by designating a command file for the earth meter to use.

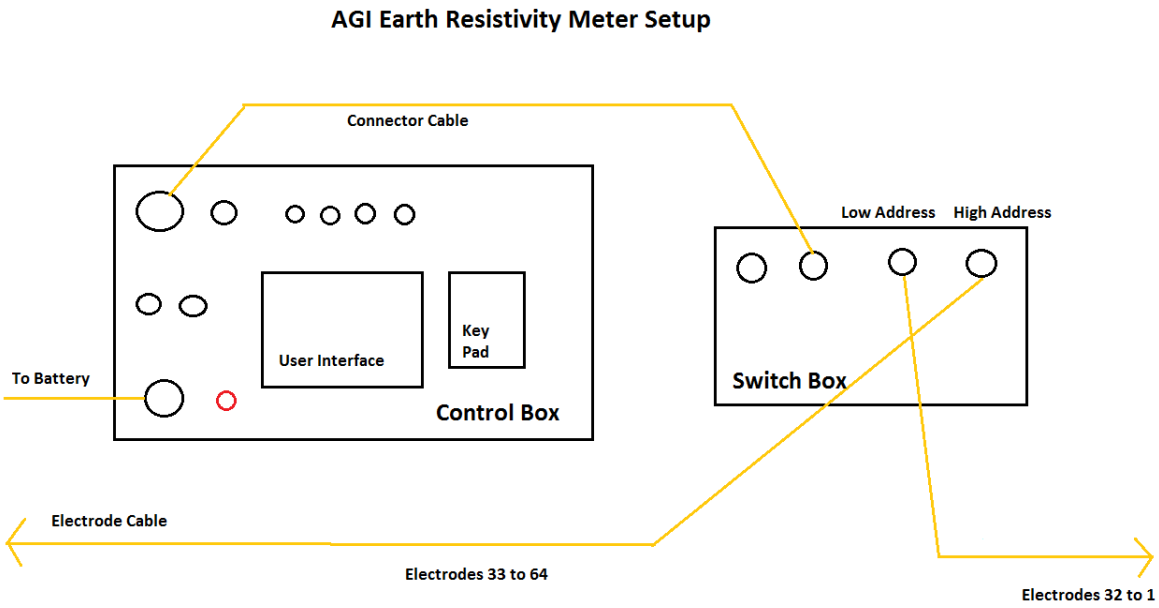

Figure 1-6. AGI Earth Resistivity Meter Setup. This is the basic set up for a 64 electrode - resistivity survey. Notice that both the switch box and control box are located in the middle of the transect between electrodes 32 and 33.

Sixth is data collection, which entails initiating the survey and waiting for the control box it collect the data. Collection time is dependent on the model of earth meter, as well as the number of electrodes used. For the AGI Supersting R8 with 64 electrodes in a Dipole-Dipole array, data collection time is approximately 36 minutes. This determines the highest possible temporal resolution for time-lapse studies. For example, if 4 – 5 surveys are desired over the duration of a 2-hour rain event, the maximum survey time should be around a half hour. Finally, once the survey is complete the earth meter will save the data file automatically and the unit may be turned off and dismantled. For a more thorough explanation of electrical resistivity theory, please refer to Herman, 2001.

1.2.2 Data Inversion

The primary output of an ERI survey is a tomogram, which is a map of subsurface resistivity. The ERI survey collects only apparent resistivity and apparent depth which then must be transformed via inversion to determine actual resistivity and actual depth in the subsurface (Travelletti et al., 2012). Apparent resistivity is a weighted average of the resistance of all of the layers current has traveled through between electrodes (Herman, 2001). Actual resistivity is an inherent property of the subsurface fluid and material. The data file from the earth meter (apparent resistivity) is inverted with an inversion software such as AGI's EarthImager. The software iteratively solves for system parameters and converges on the most likely solution. Two inversion methods are covered here, individual resistivity inversions and time-lapse inversion. Individual resistivity inversions reveal the subsurface structure at one given point in time while time-lapse inversions show only a progression of changes in the subsurface through time.

Time-lapse inversion is an extension of individual resistivity inversions in which only the difference between temporally sequential surveys (tomograms) is calculated. A control survey tomogram is used as the original resistivity of the system. This is normally the survey that is taken earliest in time. Then numerous monitor surveys are listed sequentially. Time-lapse inversion occurs by inverting the first monitor survey with respect to the control tomogram, and so on through the monitor surveys (AGI, 2009). The resulting tomograms show only changes in the subsurface through time (% difference). Because infiltrating water causes an increase in electrical conductivity in the subsurface (rather than an increase in resistivity), AGI creates time-lapse tomograms that show changes in electrical conductivity rather than electrical resistivity. Conductivity percent difference is calculated as the subsequent conductivity minus the control conductivity, divided by the control conductivity (AGI, 2009).

Data filtering is the best way to lower root mean square error (RMSE) and L2-norm errors (sum of the squared weighted data errors (AGI, 2009)) after the first inversion (Oursingbe et al., 2012; Travelletti et al., 2012). Misfit points are deviations from the model's solution and are caused by poor electrode-earth connection, as well as subsurface characteristics such as an electrode being too close to a boulder or large void space. It is important to establish a balance between reducing error and removing so much data as to be left with ideal but unrealistic results. This is done by using the original inversion output, with all of the positive data points (negative data points are erroneous and automatically removed by the software), and removing data with greater than 50% misfit via the EarthImager calculated "Data Misfit Histogram" (AGI, 2009), removed data should not be greater than 20% of the total number of data points.

1.2.3 Relevant applications

Electrical resistivity imaging is not a new technology, rather the novelty of this study was to apply ERI in a new landscape type, the surface coal mining valley fill, and use it to monitor preferential flow. ERI has been used previously to monitor both matrix and preferential flow; however it has most often been in conjunction with other sampling techniques to confirm results. There are only a couple known instances in which ERI has been deployed in a mine-related landscape; neither of which were designed or able to visualize preferential flow paths. ERI has also been used to monitor subsurface mixing. This literature review steps through the earlier studies that cumulated in the current possibility of using ERI as a standalone hydrologic investigation technique.

ERI has been used to monitor subsurface tracer plumes since the mid 1990's (White, 1994; Osiensky and Donaldson, 1995; Morris et al., 1996), however computing power starting in the early 2000's has allowed for more exact qualitative (Daily et al 1995; French, 2002) and quantitative (Slater et al., 2002) hydrologic interpretations with the latter still requiring a secondary data set for calibration. ERI was used in conjunction with a convection-dispersion model to monitor a sodium bromide (NaBr) solute plume in an unconfined aquifer (Kemna et al., 2002). Similarly, ERI measurements have been used to calibrate an end-member mixing analysis (EMMA) of karst conduit and matrix water (Meyerhoff et al., 2013). Water deficit measurements collected via ERI was compare to time-domain reflectometry (TDR) in a sandy-

shale slope. TDR and ERI measurements matched up well, and it was concluded that ERI is an accurate way to monitor soil matrix moisture (Brunet et al., 2009).

Recently, ERI studies have become accurate enough to be relied on in more complex investigations. ERI was successfully used to characterize drainage pathways beneath the disappearing Mountain Lake, VA (Roningen and Burbey 2012). The drainage path was found to be disconnected from the current stream bed and was instead located along a fault at the Eastern Continental Divide (Figure 1-8). ERI has also been used numerous times to investigate hydrologic flow paths associated with streams. One of the advantages for streams is that ERI removes the need to interpolate between point measurements which has allowed for seamless and accurate mapping of in-stream alluvial sediment extent (Crook et al, 2008). ERI was used to monitor the rate and extent of solute transport in the hyporheic zone (Ward, 2010) and to monitor migration of a conductive tracer through floodplain macropores (Menichino et al., 2014). The success of these studies once again shows the capability of electrical resistivity to map preferential flow paths.

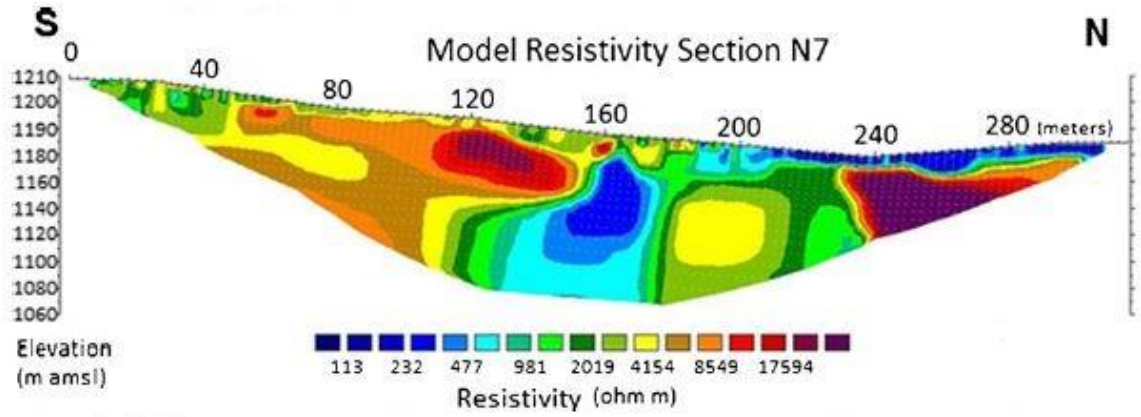

Figure1-7. Tomogram of Mountain Lake Drain (Roningen and Burbey 2012). This image shows the less resistive surface water seeping out in a location (center, blue) that is disconnected from the stream channel (upper right, blue).

The prior study closest to the methods used for this thesis is Travelletti et al. (2012) in which infiltration and subsurface flow were tracked through a clay-shale landslide. The authors used ERI and an artificial rainfall experiment to monitor the advancing wetting front for over 60 hours. Both individual resistivity inversion and time-lapse inversions were used, with primarily time-lapse inversion being used for the hydrologic analysis. A dipole-dipole array was used, as it is known for accurate resistivity measurements. Three inversion constraints (damped least-squares, least-squares smoothness, and robust smoothness) were tested, and it was found that a damped least-squares inversion constraint resulted in the least amount of uncertainty. A sensitivity study on temperature concluded that error induced by temperature variation is minimal below 0.5 meters depth into the surface. They found that the wetting front reaches steady state after 21 hours of sprinkling and were able to visualize the flow direction along with two preferential flow paths, represented by areas where constant resistivity was reached quickly,

in the landslide material (Figure 1-19). ERI was successfully used to track water movement through a disturbed landscape without a secondary measurement for comparison.

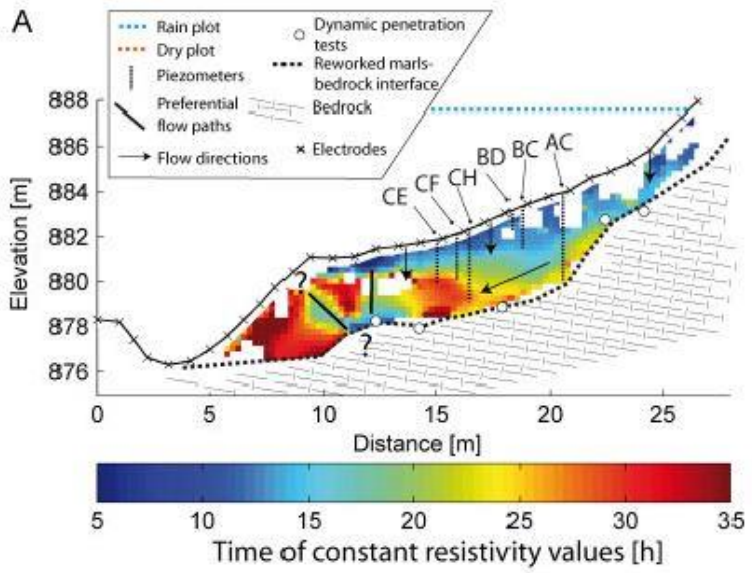

Figure 1-8. Tomogram of Preferential Flow Path in Landslide (Travelletti et al., 2012). This image shows multiple zones of where constant resistivity was reached quickly, interpreted as preferential flow paths (black line segments). It also shows the movement direction of the wetting front.

ERI has only been documented twice on mine-disturbed landscapes. The first comes from an extensive, permanent ERI based monitoring system of a capped waste rock repository in the shape of a valley fill. The monitoring system was needed to evaluate the efficacy of a new cap design in keeping water away from acid rock drainage (ARD) generating material. Although this conference paper does not specify specific inversion techniques it was able to show three months of moisture progression beneath the fill (Wangerud et al., 2006). The other mine-related ERI study was done on a 50,000 square meter, 25 meter high spoil pile in France, rather than a VF. Investigation methods included ERI, ground penetrating radar, and electromagnetic conductivity. ERI successfully delineated various subsurface features, including layers of compaction aboce unconsolidated material, however there was no hydrologic analysis (Anterrieu et al., 2010).

1.3 References

AGI, (2009). Instruction Manual for EarthImager 2D Version 2.4.0 Resistivity and IP Inversion Software. Advanced Geosciences, Inc. Austin, TX, USA.

Anterrieu, O., M. Chouteau, and M. Aubertin (2010), Geophysical characterization of the large-scale internal structure of a waste rock pile from a hard rock mine, *Bulletin of Engineering Geology and the Environment, 69,* 533-548, doi:10.1007/s10064-010-0264-4.

Bernhardt, E. S., and M.A. Palmer (2011), The environmental costs of mountaintop mining valley fill operations for aquatic ecosystems of the Central Appalachians, *Ann. N.Y. Acad. Sci. 1223,* 39–57, doi:10.1111/j.1749-6632.2011.05986.x.

Bonta, J. V., C. R. Amerman, T. J. Harlukowicz, and W. A. Dick (1997), Impact of surface coal mining on three Ohio watersheds—Surface water hydrology, *J. Am. Water Resour. Assoc., 33,* 907–917.

Bonta, J.V. (2005), Challenges in conducting hydrologic and water quality research in drastically disturbed watersheds, *J. Soil Water Conserv, 60,* 121–133.

Brunet, P., R. Clément, and C. Bouvier (2010), Monitoring soil water content and deficit using Electrical Resistivity Tomography (ERT) – A case study in the Cevennes area, France, *J. Hydrol., 380*(1–2), 146–153, doi:10.1016/j.jhydrol.2009.10.032.

Cormier, S. M., S. P. Wilkes, and L. Zheng (2013), Relationship of land use and elevated ionic strength in Appalachian watersheds, *Environ. Toxicol. Chem., 32*(2), 296–303, doi:10.1002/etc.2055.

Coscia, I., N. Linde, S. Greenhalgh, T. Gunther, and A. Green (2012), A filtering method to correct time-lapse 3D ERT data and improve imaging of natural aquifer dynamics, *J. Appl. Geophys.80,* 12–24, doi:10.1016/j.jappgeo.2011.12.015.

Crook N., A. Binley, R. Knight, D. A. Robinson, J. Zarnetske, and R. Haggerty (2008), Electrical resistivity imaging of the architecture of substream sediments, *Water Resources Research, 44,* 1-11.

Dahlin, T., and B. Zhou (2004), A numerical comparison of 2D resistivity imaging with 10 electrode arrays, *Geophys. Prospect. 52,* 379–398.

Daily, W.D., A. L. Ramirez, D. J. LaBrecque, and W. Barber (1995), Electrical resistance tomography experiments at the Oregon Graduate Institute, *J. Appl. Geophys. 33*, 227–237.

Daniels, W. L., and C. E. Zipper (1997), Creation and management of productive minesoils, *Virginia Cooperative Extension, pub 460-121.*Virginia Polytehnic Institute and State University, Blacksburg, VA.

Evans, D. M., C. E. Zipper, E. T. Hester, and S. H. Schoenholtz, (2015) Hydrologic effects of surface coal mining in Appalachia (USA). *J. Am. Water Resour. As.,(In press)*

Evans, D. M., C. E. Zipper, P. F. Donovan, and W. L. Daniels (2014), Long-term trends of specific conductance in waters discharged by coal-mine valley fills in central Appalachia, USA, *J. Am. Water Resour. As., 50(6),* 1449–1460, doi: 10.1111/jawr.12198.

Ferrari, J. R., T. R. Lookingbill, B. McCormick, P. A. Townsend, and K. N. Eshleman (2009), Surface mining and reclamation effects on flood response of watersheds in the central Appalachian Plateau region, *Water Resour. Res., 45*(4), n/a–n/a, doi:10.1029/2008WR007109.

French, H. K., C. Hardbattle, A. Binley, P. Winship, and L. Jakobsen (2002), Monitoring snowmelt induces unsaturated flow and transport using electrical resistivity tomography, *J. Hydrol. 267,* 273–284.

Geotomo, (2013), Rapid 2D Resistivity & IP inversion using the least-squares method, Geotomo Software. Panang, Malaysia.

Green, J., M. Passmore, and H. Childers (2000), A Survey of the Condition of Streams in the Primary Region of Mountaintop Mining/Valley Fill Coal Mining, US Environmental Protection Agency: Philadelphia, PA, USA.

Griffith, M. B., S. B. Norton, L. C. Alexander, A. I. Pollard, and S. D. LeDuc (2012), The effects of mountaintop mines and valley fills on the physicochemical quality of stream ecosystems in the central Appalachians: A review, *Sci. Total Environ.*, *417–418*, 1–12, doi:10.1016/j.scitotenv.2011.12.042.

Guebert, M. D., and T. W. Gardner (2001), Macropore flow on a reclaimed surface mine: infiltration and hillslope hydrology, *Geomorphology*, *39*(3–4), 151–169, doi:10.1016/S0169-555X(00)00107-0.

Hartman, K. J., M. D. Kaller, J. W. Howell, J. A. Sweka (2005), How much do valley fills influence headwater streams?, *Hydrobiologia 532*, 91–102.

Hawkins, J. W. (2004), Predictability of Surface Mine Spoil Hydrologic Properties in the Appalachian Plateau, *Ground Water*, *42*(1), 119–125.

Hawkins, J. W., and W.W. Aljoe, (1992), Pseudokarst groundwater hydrologic characteristics of a mine spoil aquifer, *Mine Water Environ., 11(2),* 37-52.

Herman, R. (2001), An introduction to electrical resistivity in geophysics, *Am. J. Phys. 69*, 943–952, doi: 10.1119/1.1378013.

Holl, K. D. (2002), Long-term vegetation recovery on reclaimed coal surface mines in the eastern USA, *J. Appl. Ecol. 39*, 960–970.

Johnson T. C., L. D. Slater, D. Ntarlagiannis, F. D. Day-Lewis, and M. Elwaseif (2012), Monitoring groundwater-surface water interactions using time-series and time-frequency analysis of transient three-dimensional electrical resistivity changes, *Water Resour. Res. 48(W07506), 1-13*, doi:10.1029/2012WR011893.

Johnson, B. R., A. Haas, and K. M. Fritz (2010), Use of spatially explicit physicochemical data to measure downstream impacts of headwater stream disturbance. *Water Resour. Res. 46*, W09526.

Kemna, A., J. Vanderborgh, B. Kulessa, H. Vereecken (2002), Imaging and characterization of subsurface solute transport using electrical resistivity tomography (ERT) and equivalent transport models, *J. Hydrol., 267,* 125-146.

Kirk, E. J., R. Maggard (2004), Long-term downstream impacts of surface mining and valley fill construction to benthic macroinvertebrates and water quality, in Proceedings of the Joint Conference of 21st Annual Meetings of the American Society of Mining and Reclamation and 25th West Virginia Surface Mine Drainage Task Force Symposium, Morgantown, WV. Lexington, KY: American Society of Mining and Reclamation.

Lindberg, T. T., E. S. Bernhardt, R. Bier, A. M. Helton, R. B. Merola, A. Vengosh, and R. T. D. Giulio (2011), Cumulative impacts of mountaintop mining on an Appalachian watershed, *P. Natl. Acad. Sci. USA*, *108*(52), 20929–20934, doi:10.1073/pnas.1112381108.

McCormick, B. C., K. N. Eshleman, J. L. Griffith, and P. A. Townsend (2009), Detection of flooding responses at the river basin scale enhanced by land use change, *Water Resour. Res.*, *45*(8), n/a–n/a, doi:10.1029/2008WR007594.

Menichino, G. T., A. S. Ward, and E. T. Hester (2014), Macropores as preferential flow paths in meander bends. *Hydrol. Process., 28,* 482-495.

Merricks, T. C., D. S. Cherry, C. E. Zipper, R. J. Currie, and T. W. Valenti (2007), Coal-mine hollow fill and settling pond influences on headwaterstreams in southern West Virginia, USA, *Environ. Monit. Assess.*, 129,359–378.

Messinger, T. (2003), Comparison of storm response of streams in small, unmined and valley-filled watersheds, 1999 – 2001, Ballard Fork, WV, Office of Surface Mining, Reclamation, and Environmen,. Water-resources Investigation Report 02-4303.

Messinger, T., and K. S. Paybins (2003). Relations between Precipitation and Daily and Monthly Mean Flows in Gaged, Unmined and Valley-Filled Watersheds, Ballard Fork, West Virginia, 1999–2001, US Geological Survey: Charleston, WV, USA, Water-resources Investigation Report 2003-4113.

Meyerhoff, S. B., R. M. Maxwell, A. Revil, J. B. Martin, M. Karaoulis, and W. D. Graham (2014), Characterization of groundwater and surface water mixing in a semiconfined karst aquifer using time-lapse electrical resistivity tomography, *Water Resour. Res., 50*, 2566–2585, doi:10.1002/ 2013WR013991.

Miller, A. J., and N. P. Zegre (2014). Mountaintop Removal Mining and Catchment Hydrology. *Water*, *6,* 472-499. doi:10.3390/w6030472

Morris, M., J. S. Rønning, and O. B. Lile, (1996), Geoelectric monitoring of a tracer injection experiment: modeling and interpretation, *Eur. J. Environ. Engng Geophys. 1*, 15–34.

Negley, T. L., and K. N. Eshleman (2006), Comparison of stormflow responses of surface-mined and forested watersheds in the Appalachian Mountains, USA, *Hydrol. Process., 20*(16), 3467–3483, doi:10.1002/hyp.6148.

Osiensky, J. L., and P. R. Donaldson (1995), Electrical flow through an aquifer for contaminant source leak detection and delineation of plume evolution, *J. Hydrol. 169*, 243–263.

Palmer, M. A., E. S. Bernhardt, W. H. Schlesinger, K. N. Eshleman, E. Foufoula-Georgiou, M. S. Hendryx, A. D. Lemly, G. E. Likens, O. L. Loucks, M. E. Powers, P. S. White, and P. R. Wilcock (2010), Mountaintop Mining Consequences, *Science, 327*(5962), 148–149, doi:10.1126/science.1180543.

Parker, J. M., (2013), Effect of Various Saturation Levels, Leaching Solution pH, and Leaching Cycle on Electrical Conductivity of Coal Mine Spoil Leachate (Master's Thesis), Virginia Polytechnic and State University, Blacksburg VA, USA.

Paybins, K. S., T. Messinger, J. H. Eychaner, D. B. Chambers, and M. D. Kozar (2000), Water quality in the Kanawha-New River Basin, West Virginia, Virginia, and North Carolina, 1996-98. U.S. Department of the Interior, U.S. Geological Survey, Washington D.C.

Peng, S. S. (2000), Mountaintop removal controversy slows West Virginia coal mining. *Min. Eng., 52*, 53–58.

Phillips, J. D. (2004), Impact of surface mine valley fills on headwater floods in eastern Kentucky, *Environ. Geol. 45*, 367-380, doi:10.1007/s00254-003-0883-1.

Pond, G. J. (2010). Patterns of Ephemeroptera taxa loss in Appalachian headwater streams (Kentucky, USA), *Hydrobiologica, 641,* 185-201, doi: 10.1007/s10750-009-0081-6.

Pond, G. J., M. E. Passmore, F. A. Borsuk, L. Reynolds, and C. J. Rose (2008), Downstream effects of mountaintop coal mining: comparing biological conditions using family- and genus-level macroinvertebrate bioassessment tools, *J. N. Am. Benthol. Soc.*, *27*(3), 717–737, doi:10.1899/08-015.1.

Puente, C., and J. T. Akins (1989), Simulation of rainfall-runoff response in mined and unmined watersheds in the coal areas of West Virginia, U.S. Geological Survey, U.S. Bureau of Land Management, Washington D.C., Water Supply Paper 2298.

Roningen J., and T. J. Burbey (2012), Hydrologic controls on lake level: a case study at Mountain Lake, Virginia, USA, *Hydrogeol. J. 20*, 1149-1167, doi:10.1007/s10040-012-0859-x.

Saylor, K. L. (2008), Land Cover Trends Project: Central Applachians. U.S. Department of the Interior, U.S. Geological Survey. Washington, DC. Retrieved from: http://landcovertrends.usgs.gov/east/eco69Report.html.

Seaton, W. J., and T. J. Burbey (2002), Evaluation of two dimensional resistivity methods in fractured crystalline-rock terrane, *J. App. Geophys., 51*, 21-41.

Slater, L., A. Binley, R. Vertseeg, G. Cassiani, R. Birken, and S. Sandberg (2002), A 3D ERT study of solute transport in a large experimental tank, *J. App. Geophys. 49*, 211-229.

Travelletti, J., P. Sailhac, J. P. Malet, G. Grandjean, and J. Ponton (2012), Hydrological response of weathered clay-shale slopes: water infiltration monitoring with time-lapse electrical resistivity tomography, *Hydrol. Process., 26*(14), 2106–2119. doi:10.1002/hyp.7983

U.S. Congress, (1977), Surface Mining Control and Reclamation Act, US Congress: Washington, D.C.

U.S. Environmental Protection Agency (1999) Rapid Bioassessment Protocols for Use in Wadeable Streams and Rivers, *EPA 841-B-99-002*,Office of Water, Washington, D.C.

U.S. Environmental Protection Agency (2010), A Field-based Aquatic Life Benchmark for Conductivity in Central Appalachian Streams (External Review Draft), EPA-600-R-10-023A, Washington, D.C.

U.S. Environmental Protection Agency (2011), The Effects of Mountaintop Mines and Valley Fills on Aquatic Ecosystems of the Central Appalachian Coal Fields. *EPA 600-R09-138F*, Office of Research and Development, Washington, D.C.

Wangerud, K., R. Versteeg, G. Heath, R. Markiewicz, and A. Richardson (2006), Insights into hydrodynamic and geochemical processes in a valley fill ARD and waste rock repository from an autonomous multi-sensor monitoring system, Proceedings of the 7th International Conference of Acid Rock Drainage, St. Luis MO, *ASMR.*

Ward, A. S., M. N. Gooseff, and K. Singha (2010), Characterizing hyporheic transport processes - Interpretation of electrical geophysical data in coupled stream-hyporheic zone systems during solute tracer studies, *Adv. Water Resour., 33*,1320-1330.

West Virginia Department of Environmental Protection, Flood Advisory Task Force, (2002), Runoff analyses of Seng, Scrabble, and Sycamore Creeks, Part 1, retrieved from: http://www.dep.state.wv.us/Docs/1593Part%20I.pdf

White, P. A. (1994), Electrode arrays for measuring groundwater flow direction and velocity, *Geophysics 59*, 192–201.

Wiley, J. B., and F. D. Brogan (2003), Comparison of Peak Discharges Among Sites with and without Valley Fills for the July 8–9 2001, Flood in the Headwaters of Clear Fork, Coal River Basin, Mountaintop Coal-Mining Region, Southern West Virginia, U.S. Department of the Interior, U.S. Geological Survey: Charleston, WV, USA.

Wiley, J. B., R. D. Evaldi, J. H. Eychaner, and D. B. Chambers, (2001), Reconnaissance of Stream Geomorphology, Low Streamflow, and Stream Temperature in the Mountaintop Coal-Mining Region, Southern West Virginia, 1999–2000, US Geological Survey: Charleston, WV, USA.

Wunsch, D. R., J. S. Dinger, and C. D. R. Graham (1999), Predicting ground-water movement in large mine spoil areas in the Appalachian Plateau, *Int. J. Coal Geol. 41*, 73–106.

Zégre, N. P., A. Maxwell, and S. Lamont (2013), Characterizing streamflow response of a mountaintop-mined watershed to changing land use, *Appl. Geogr., 39*, 5–15.

Zégre, N., A. J. Miller, A. Maxwell, and S. Lamont (In Press) Multi-scale analysis of hydrology in a mountaintop mine impacted watershed. *J. Am. Water Resour. Assoc.*

Zipper, C. E., J. A. Burger, J. G. Skousen, P. N. Angel, C. D. Barton, V. Davis, and J. A. Franklin, (2011), Restoring forests and associated ecosystem services on Appalachian coal surface mines. *Environ. Manage. 47*, 751–765, doi:10.1007/s00267-011-9670-z.

Chapter 2 - Electrical Resistivity Imaging Of Preferential Flow through Surface Coal Mine Valley Fills

In Preparation for Publication in Hydrological Processes

Breeyn M. Greer, Erich T. Hester*, Thomas J. Burbey, and Carl E. Zipper

** Corresponding Author:*

Erich T. Hester

The Charles E. Via, Jr. Department of Civil and Environmental Engineering
Virginia Polytechnic and State University
220-D Patton Hall
Blacksburg, VA 24061

Email: ehester@vt.edu
Phone: 540-231-9758

Other Authors:

Breeyn M. Greer

The Charles E. Via, Jr. Department of Civil and Environmental Engineering
Virginia Polytechnic and State University
220-D Patton Hall
Blacksburg, VA 24061

Thomas J. Burbey

Department of Geosciences
Virginia Polytechnic and State University
3409-A Derring Hall
Blacksburg VA, 24061

Carl E. Zipper

Department of Crop and Soil Environmental Siences
Virginia Polytechnic and State University
363 Smyth Hall
Blacksburg VA, 24061

2.1. Introduction

Mountaintop removal mining (MTRM), a form of surface coal mining, originated in the 1960's due to increased demand for energy combined with more powerful earth moving equipment (US EPA, 2011). Surface mining in central Appalachia, including MTRM, involves removal of rock materials (overburden) and coal from the surface to depths of up to 300 m (Peng, 2000) which results in drastic and often permanent changes to the local topography, soil structure, and land cover (Miller and Zegre, 2014). During reclamation, excess overburden caused by the expansion of bedrock during the removal process is placed in adjacent valleys, creating valley fills (VF), and covering headwater streams.

In the United States, MTRM is primarily confined to the central Appalachian coalfield region consisting of eastern Kentucky, southern West Virginia, northeastern Tennessee, and southwest Virginia (Lindberg et al., 2011; US EPA 2011). Over 600,000 hectares have been mined eastern USA's Appalachian coalfield (Zipper et al. 2011) such that surface coal mining has caused large-scale land use change throughout Appalachia (Salyer, 2008). The central Appalachian coalfield is home to many headwater streams, 4,000 km of which have been buried by valley fills (US EPA, 2011). Due to its age (having escaped glaciation in the last ice age), climate, and topography, this region has very high aquatic species richness in streams and rivers (Bernhardt and Palmer, 2011). There is a direct relationship between extent of upstream mining disturbance and loss of Ephemeroptera (mayfly) species richness and relative abundance (Pond et al., 2008).

Both water quality and hydrologic changes result from Appalachian surface coal mining. Water quality changes include increased pH and total dissolved solids, and may include increased concentrations of trace elements such as Se (Hartman et al., 2005; Pond et al., 2008; Palmer et al., 2010; Bernhardt and Palmer, 2011; Lindberg et al. 2011; Griffith et al., 2012; Pond et al. 2014; Timpano et al. 2015). Elevated TDS is common and widespread in Appalachian coalfield streams (Griffith et al., 2012). Elevated TDS is believed to cause biotic effects in freshwater streams by inducing osmoregulatory stresses (Pond et al., 2008; Bernhardt and Palmer, 2011). High TDS occurs in mine water discharges as a result of large quantities of broken rock undergoing accelerated weathering via exposure to water and air. TDS is often measured through its surrogate, specific conductance (SC). Natural background SC for headwater streams in the Appalachian coalfield region is generally <200 µS/cm, but SCs in mining affected streams are often far higher, up to 2500 µS/cm or greater (Hartman et al. 2005; Merricks et al. 2007; Pond et al. 2008; Lindberg et al., 2011; Pond et al. 2014; Timpano et al. 2015). Thresholds for biotic effects in Appalachian streams have been reported in the range of 300 to 500 µS/cm (Pond et al., 2008; Bernhardt et al., 2012; Cormier et al., 2013a).. Specific conductance in Appalachian streams has been shown to increase with increasing area of active mining activities in the watershed, and to be strongly correlated to VF extent (Lindberg et al. 2011; Cormier et al., 2013b). SC has also been shown to be a good predictor of other solutes in the water such as sulfates, bicarbonate, calcium, and magnesium (Lindberg et al., 2011; Timpano et al. 2015).

Studies have shown that mining disturbances cause hydrologic changes (Miller and Zegre 2014; Evans et al. 2015), yet the relationship between reconstructed landscape structure, hydrology, and water quality remains unclear. Common hydrologic changes include flashier stormwater

runoff hydrographs with increased tailing (Guebert and Gardner, 2001; Messinger, 2003; Negley and Eshleman, 2006; McCormick et al., 2009), increased volume and duration of baseflow (Green et al., 2000; Wiley et al., 2001; Messinger and Paybins, 2003; Zegre et al., 2014), and the formation of unnatural flow paths over and through the mined landscape (Miller and Zegre 2014; Evans et al. 2015). Unnatural flow paths occur due to the large volumes of fractured rock that comprise mine spoil fills, which contain a variety of rock sizes and void spaces. Mine-soil surface infiltration properties are also highly variable (Evans et al. 2015). Water may infiltrate minimally due to a highly compacted surface layer (Simmons et al. 2008), or may infiltrate more rapidly (Guebert and Gardner 2001). Within the mine-spoil fills, water may flow infiltrates along preferential flow paths that are influenced by voids (previously referred to as pseudokarst, Caruccio and Geidel 1984, or conduits, Hawkins and Aljoe, 1992). The surface and subsurface interfaces that control stormflow partitioning have been referred to as control points (Evans et al., 2015). Preferential flow has previously been surmised by stitching together point measurements, rather than observed directly. The exact flow processes of infiltrated stormwater and the mechanisms through which effluent stream water becomes elevated in SC is largely unknown.

Valley Fills are the mining-related structure most strongly correlated with downstream water quality effects (Cormier et al., 2013b). Therefore, if TDS production could be limited in the valley fill, downstream water quality may improve. Due to rocky terrain and limited access to all parts of mine-impacted watersheds, previous hydrologic studies have focused on inputs and outputs, with only point measurements from groundwater wells and falling-head tests on the valley fill (Hwakins and Aljoe, 1992; Hawkins, 1998, 2004; Wunsh et al., 1999). This approach views the interior of fills as a black box and does not clarify the flow regime where TDS is acquired. By contrast, integrative techniques that can gather spatially contiguous data at various scales on the storage, transport, and flow of water through spoil hold promise to illuminate processes occurring within the valley fill structure (Miller and Zegre, 2014). Geophysical techniques such as electrical resistivity imaging (ERI) present a possible solution. ERI is a non-invasive, continuous subsurface mapping technique that is used to characterize subsurface lithology and water movement spatiotemporally through variation in electrical resistivity.

ERI has been used to monitor subsurface tracer plumes since the mid 1990's (White, 1994; Osiensky and Donaldson, 1995; Morris et al., 1996), however increased computing power starting in the early 2000's allowed more exact qualitative (Daily et al 1995, French et al., 2002; Rugh and Burbey, 2008) and quantitative (Slater et al., 2000; Brunet et al., 2009) hydrologic interpretations. The latter generally requires a secondary data set for calibration (e.g., French et al., 2002; de Bari et al., 2011) or pairing with a mixing model (e.g., Kemna et al., 2002; Meyerhoff et al., 2013) for validation. Fewer ERI studies have investigated preferential flow paths, but Menichino et al. (2014) imaged preferential flow through floodplain macropores and Travelletti et al. (2012) imaged preferential flow through a clay-shale landslide. We are aware of few instances where ERI was deployed in a mine-related landscape, including one that captured general moisture movement (Wangerud et al., 2006) and another that imaged mine spoil structure (Anterrieu et al., 2010) Nevertheless, neither study was done on a valley fill, and neither visualized preferential flow paths.

The objectives of our study were to deploy ERI in a novel setting to track stormwater as it moves through a valley fill. In particular, we sought to develop an approach to successfully use ERI in this setting to 1) image the valley fill's geologic structure; 2) image movement of subsurface stormflow within the fill; and (3) compare the valley fill's image structure to a filled highwall slope and an unmined hillslope,

2.2. Site Description / Background Data

The field site is a large surface coal mine valley fill located in southwest Virginia. Geology in this area is from the Pennsylvanian era, with this particular unit known as the Wise Formation (USGS, 2013). The fill is approximately 6 years old, and composed primarily of gray and brown sandstone. A tiered design consisting of a series of slopes and benches was used for construction (Figure 2-1). Areas of large boulders intended to quickly conduct surface runoff downslope (i.e. side drains) are present on each side. There is also likely a subsurface center drain where the original headwater stream bed was, however this is not confirmed. All such drains transmit water to a perennial effluent stream that emanates from the toe of the fill and drains to a small pond at approximately 40 m distance. The fill surface is approximately 150 m wide at the widest point and 350 m long. The land surface rises 65 m in elevation along the valley fill's length. The watershed area draining to valley fill toe is approximately 23 hectares and, except for slopes immediately adjacent to the valley fill, is 100% mined.

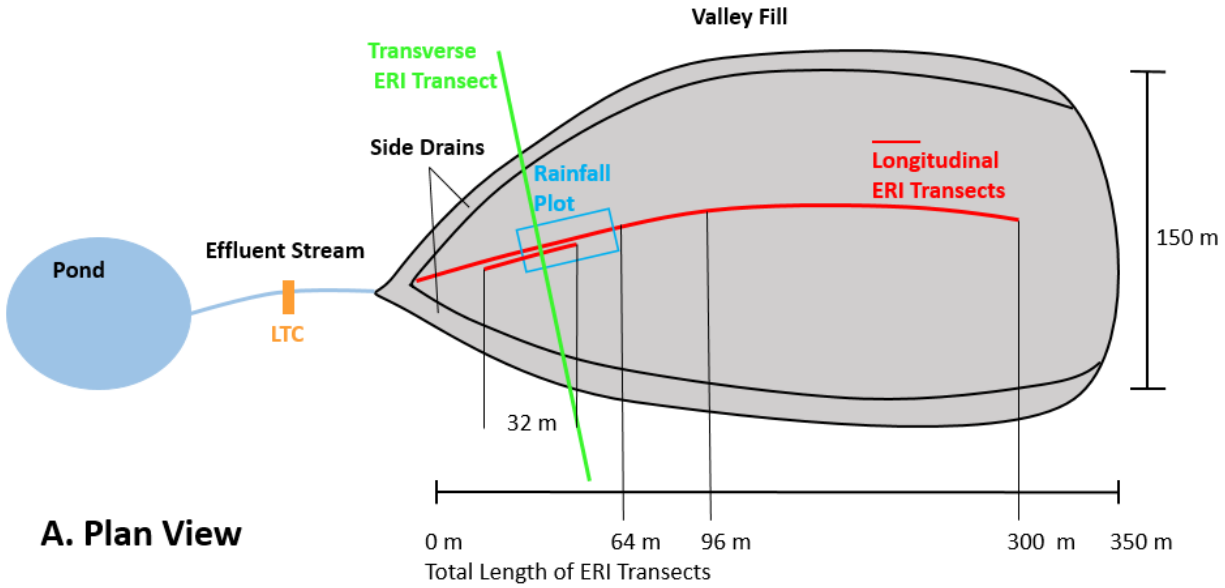

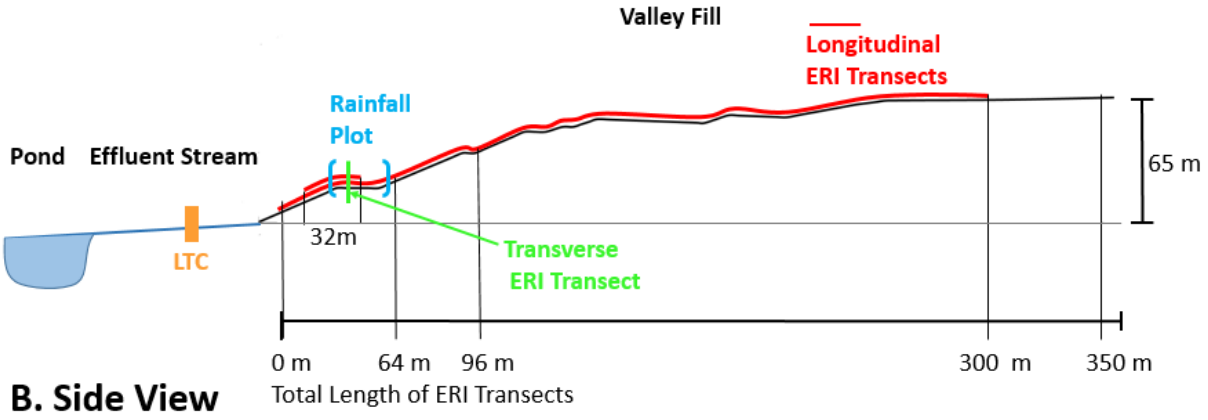

Figure 2-1. Schematic of valley fill with ERI transects. Panel A is a plan view of the valley fill surface and Panel B is a side view. Shown are location of the sediment pond, effluent stream, LTC (level. temperature, conductivity meter), rainfall plot, and ERI transects. Total length of ERI transects correspond with experiments in Table 1. Not drawn to scale.

We collected background data on water level and SC in the effluent stream to understand hydrologic and water quality cycles at the site. We installed a Solinst Levelogger Junior 3001 (Toronto, Canada) in the effluent stream and logged water level, temperature, and specific conductance (LTC) every 10 minutes starting on November 8th, 2013 and running until July 23rd, 2014 (Figure 2-2), when data collection was disrupted due to effluent stream channel reconstruction. Data collection after July 23rd was unreliable due to instability of the new channel. SC is elevated in the stream, consistent with effects of MTRM / VF activities. With increasing water level there is often a decrease in SC, consistent with a pattern of high SC at baseflow and lower SCs when diluted by stormflow.

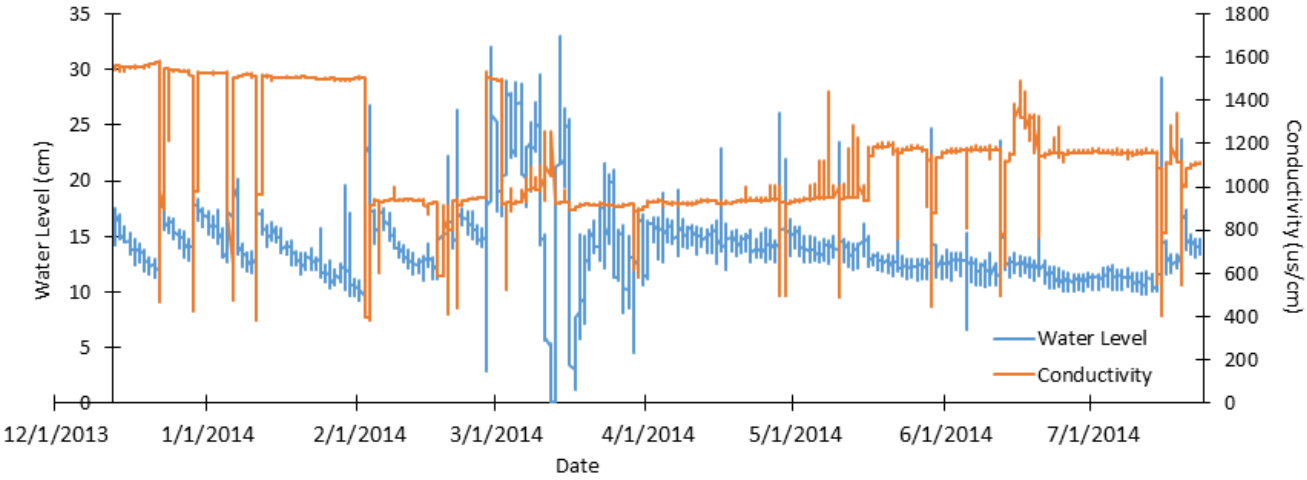

Figure 2-2. Water level and specific conductance versus time, November 8th through July 23rd, 2014. Data were collected in the effluent stream every 10 minutes.

Starting in June 2014, we also collected precipitation data on site with a Texas Electronics Inc. TR5251 (Dallas, TX) tipping bucket and Campbell Scientific Inc. CR 1000 data logger (Logan, UT), (Figure 2-3). This instrument documented antecedent moisture conditions for the ERI surveys.

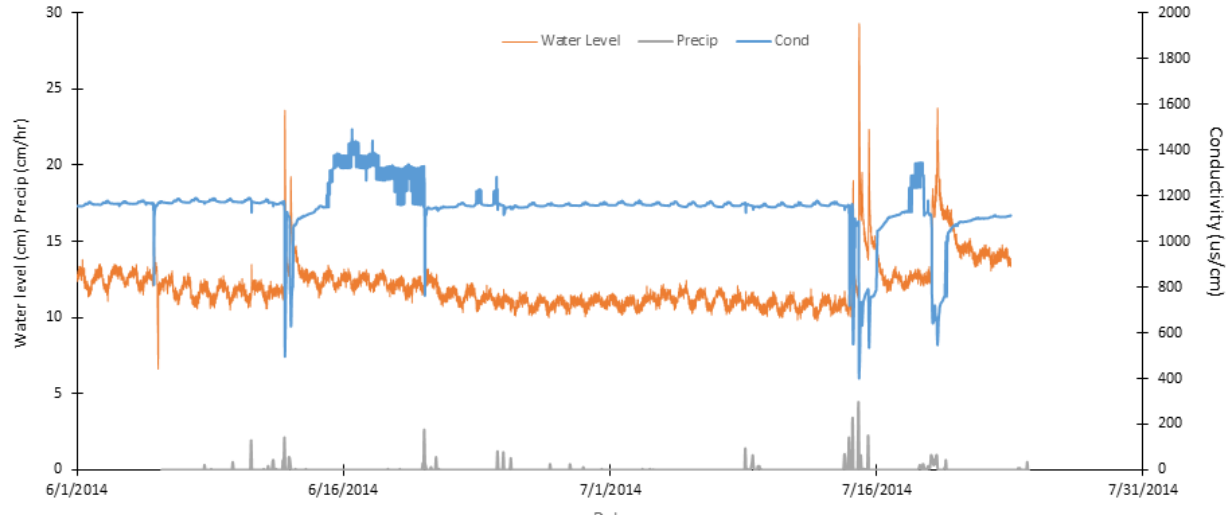

Figure 2-3. Precipitation data at the valley fill and water level and specific conductance in the effluent stream, June 1st through July 23rd, 2014. The relationship between precipitation, increase in water level, and a decrease in conductivity is evident.

2.3. Methods

Our study comprised three phases: artificial rainfall experiments, field collection of electrical resistivity surveys, and electrical resistivity data inversion to create ERI images.

2.3.1 Artificial Rainfall Experiments

Rainfall experiments occurred on a 10 m by 30 m plot on the first level bench up the fill from the effluent stream (Figure 2-1). This bench is 17 vertical meters above and 40 lateral meters away from the stream. The 20 m wide bench was chosen as the rainfall plot in hopes that the minimal slope would facilitate infiltration. We pumped high EC pond water up to the bench with a Koshin SERM-50V centrifugal pump with a Mitsubishi GM182 4-cycle engine from PumpBiz Inc. (Northbrook, IL). The water was 900 – 1400 uS/cm, (7 – 12 Ohm-m), and SC was recorded every hour to ensure consistency for the duration of an individual rainfall experiment. The pump has a capacity of 0.005 m^3/s at 413.7 kPa (80 GPM at 60 psi) and a maximum head of 90 meters. We varied the pump speed slightly between experiments in order to keep the extent of the artificial rainfall primarily within the plot boundaries. Water was pumped through 100 meters of 5 cm diameter fire hose and distributed through a sprinkler system consisting of four Melanor (619-344) oscillator sprinklers in parallel, connected to the fire hose with 5 to 15 meters of standard garden hose.

We monitored three rain gages within the plot during rainfall experiments. Simulated precipitation rates varied from 1.2 cm/hr to 2.5 cm/hr depending on the location within the plot

and the pump speed. Precipitation rate was consistently higher than infiltration capacity of the soil material as we observed ponding on the surface after one hour. The initial soil moisture conditions varied for each study from no natural or artificial precipitation in the previous week, to a 16-hour drain period just before the artificial rainfall experiment. Most experiments were done under dry conditions (at least 48 hours of no precipitation prior). Only one rainfall experiment was done under wet conditions (16 hours of no precipitation prior).

2.3.2 Field Collection of Electrical Resistivity Data

We used ERI to visualize both geologic heterogeneity and resistivity (inverse of electrical conductivity) changes induced by infiltrated rainfall in the subsurface of the valley fill. ERI generates data sets known as surveys which consist of hundreds of measurements in the subsurface. A measurement is the reading of one apparent resistance at a single subsurface location. Each measurement is taken with four electrodes (one quadripole) consisting of a current (I) pair and a potential difference (V) pair (Ward et al., 2010). The order of electrodes within a quadripole is known as an array. We chose a dipole-dipole array, meaning that I is injected between two adjacent electrodes, and V is then read between two separate adjacent electrodes (Figure 2-4). We chose the dipole-dipole array because of its documented usefulness in large geophysical inverse problems where depth is valued and vertical heterogeneity is anticipated (Herman 2001, Seaton and Burbey 2002, Dahlin and Zhou, 2004). The earth meter starts the survey at intervals of one (Quadripole 1 (n=1), Figure 2-4) and moves up the transect one electrode at a time. The data level (n) indicates both the number of passes across the transect and relative depth into the subsurface (each subsequent pass is deeper). Each subsequent pass skips one more electrode (Quadripole 18 (n=2) and Quadripole 32 (n=3)) and collects fewer measurements until the final pass contains only one measurement with I_1 and V_2 being at either end of the transect (Quadripole 56, n=6). The result of all of the measurements is the survey which is used to produce an image, known as a tomogram. These images represent two-dimensional maps of electrical resistivity along a vertical slice into the subsurface beneath the transect of electrodes. A more thorough explanation of electrical resistivity theory can be found in Herman (2001).

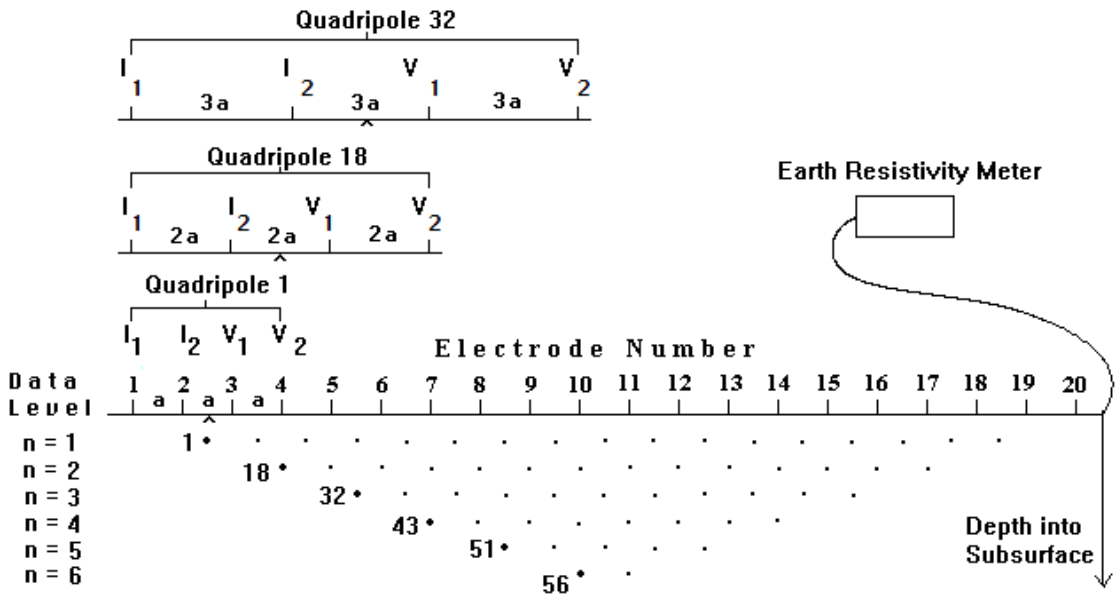

Figure 2-4. Dipole-Dipole array with data collection sequence (modified from Geotomo, 2013). The orientation of electrodes in a dipole-dipole array is I_1, I_2, V_1, and V_2. Example sequences are shown for quadripoles 1, 18, and 32. Data collection in the sequence progresses in horizontal layers of increasing depth (n=1-6) and electrode spacing.

Length and depth of tomograms are proportional such that depth is up to one fifth of the transect length (Roningen and Burbey, 2012). Spatial resolution of subsurface features increases as electrode spacing decreases because relative resolution is constant with respect to the total transect length. For each transect length an initial dry survey was taken to visualize subsurface geology and to serve as a control when detecting rainfall induced changes.

We used an Advanced Geosciences Inc. (AGI), SuperSting R8 (Austin, TX), with 64 electrodes placed between 0.5 and 5.0 meters apart (Figure 2-1). The SuperSting R8 is an eight channel earth resistivity meter (earth meter) which allows for relatively quick data collection. Because of the array chosen, the number of electrodes used, and the model of earth meter it takes 35 minutes to collect the data for one survey; thus, the highest temporal resolution possible with this instrument configuration is one survey every 35 minutes. We conducted surveys at various time intervals depending on the total duration of the rainfall experiment (Table 2-1), with the goal of having 4 to 5 surveys per experiment. We measured topography of each transect with a clinometer and created the profile terrain file, which is needed for inversion.

Table 2-1. ERI survey properties. ERI surveys varied in terms of electrode spacing, transect length, rainfall time between surveys, and dry time before rainfall onset. Total rainfall depth was calculated by averaging the final depth of the three rain gages within the rainfall plot.

Survey Series**	Date	Electrode Spacing (m)	Transect Length (m)	Rainfall Duration (hr)	Total Rainfall Depth (cm)	Time Interval Between Surveys	Pre-rainfall Dry Time *
Longitudinal (dry)	7/31/2014	5	300	N/A	N/A	N/A	4 days
Transverse (dry)	5/22/2014	3	190	N/A	N/A	N/A	4 days *
Artificial Rain 1.5m (RN4X)	7/17/2014	1.5	96	5	6.7	1:15	2 days
Artificial Rain 1.0m (RN3X)	7/11/2014	1.0	64	2:15	6.1	0:45	16 hours
Artificial Rain 0.5m (RN5X)	7/31/2014	0.5	32	2:15	4.5	0:45	4 days
Highwall (dry)	8/13/2014	2.0	128	N/A	N/A	N/A	2 days *
Natural Slope (dry)	11/15/2014	2.0	128	N/A	N/A	N/A	7 days *

* For surveys taken on dates without a weather station on site, rainfall data was taken from the NOAA weather station, Wise VA (#44-9215).
** The X in RN4X etc. signifies that there are multiple surveys in the experiment titled RN4.

We also conducted longitudinal synoptic surveys of two other land-forms to compare geologic structure with the valley fill, including a natural slope and a previously mined highwall with adjacent fill slope (Table 2-1). A filled highwall slope is formed by first mining laterally into a hillslope such that there is a vertical boundary where mining stopped (highwall). Then, fill is dumped off the top of the highwall such that it builds up and out until the final topography resembles the original topography. All three landscape types were located within 5.5 kilometers of each other to minimize geologic variability.

Electrode-earth contact is an important factor in all ERI surveys as the quality of this contact affects the quality of the data collected. Mine spoil is often composed of compacted small rock particles (soil-sized rock fragments) with interspersed large rocks, making electrode installation difficult. To ensure good electrode-earth contact, we installed electrodes carefully and completed resistance tests prior to data collection. We avoided large rocks and void spaces because both will result in artificially high resistance measurements. Once properly installed, we poured approximately a half liter of water on each electrode so that small soil pores may expand around it, increasing contact. We then completed the resistance test via the earth meter, by injecting I and reading V between concurrent electrodes all the way up the transect. Electrodes with outlying V values (relative to the other V values in the test) indicate possible poor connection. In such cases we reinstalled the electrodes and reran the resistance test.

2.3.3 Electrical Resistivity Data Inversion

The survey output from the earth meter is a file of measurements, each of which contains three elements: voltage normalized by current (V/I), apparent resistivity (ρa) and measurement geometry. We inverted this data, with the addition of the terrain data file, using AGI's EarthImager inversion software (AGI, 2009) to generate modeled resistivity (ρ) and location from which EarthImager creates a subsurface map, or tomogram. We performed inversion in two ways, individual resistivity inversions and time-lapse inversion. Individual resistivity inversions are done with no reference to other surveys and produce a tomogram which shows subsurface resistivity at one point in time (e.g., Figure 2-5, 2-6). By contrast, time-lapse inversion tomograms show only changes to the subsurface electrical conductivity between the earliest survey in a series of surveys (the control) and a subsequent survey (e.g., Figure 2-7, 2-8). Electrical conductivity percent difference from the control is displayed in the tomogram (e.g., Figure 2-7, 2-8) because the change in the subsurface due to the infiltration of high SC water is an increase in electrical conductivity, rather than resistivity. Using the control and subsequent inverted resistivities, percent difference is calculated via Equation (1):

$$\Delta\rho t = 100 * \frac{(\rho t - \rho t_0)}{(\rho t_0)} \qquad (1)$$

where ρt (Ohm-meter) is the resistivity from a subsequent survey and ρt_0 is the background resistivity from the control survey (Travelletti et al., 2012). Time-lapse tomograms have been found to be more accurate than individual resistivity tomograms because systematic errors are removed (Kemna et al., 2002; Samouëlian *et al*., 2005).

Due to the highly heterogeneous nature of valley fill material and resulting difficulty installing some of the electrodes, there was relatively high root mean square error (RMSE) and L2-norm (sum of the squared weighted data errors (AGI, 2009)) after the first inversion of each survey (Oursingbe et al., 2012; Travelletti et al., 2012). Thus, we filtered the data to remove misfit data points and effectively bring down these errors. Misfit points are deviations from the model's solution and are caused by poor electrode-earth connection, as well as subsurface characteristics such as an electrode being too near to a boulder or large void space. It is important to balance removing points to reduce error against removing too much data that leaves ideal and thus unrealistic results. We did this by using the original inversion output, with all of the data points and then removing the 10 – 20% of data that had the worst fit via the EarthImager calculated "Data Misfit Histogram" (M. Lagmanson of AGI, Personal Communication, September 11, 2014). Data with greater than 50% misfit should be removed (AGI, 2009), although by removing 10-20% of the worst fit data, remaining data often had no more than 30% misfit.

There are many inversion parameters that can be used in geophysical inverse modeling. We chose the following parameters to create a tomogram that has low RMSE and best reflects our understanding of the subsurface. We used a smoothness constrained regularized least-squares inversion algorithm with a finite element method forward model, a Cholesky Decomposition forward equation solver, and Dirichlet boundary conditions. As is standard in EarthImager's surface model, we set thickness increment and depth factors both to 1.1, meaning that modeled data level thickness increased by x1.1 incrementally with depth and the software stretches the

total available depth by x1.1 from that given by the array and transect length. This was done to optimize the output depth while maintaining resolution integrity. Setting the resolution factor to 0.2 also helped to increase resolution in areas of low sensitivity (e.g. at depth) (AGI, 2009). We used two mesh divisions, meaning that there are two model cells between each electrode pair because the dipole-dipole array is most sensitive in the short distance between electrodes (Roningen and Burbey, 2012) which can become observational error near the surface. We set the iteration stop criteria to eight inversions, maximum RMS of 3%, less than 2% RMS reduction, or L2 norm; however convergence usually occurred at a maximum of four inversions. During each successive iteration, the model uses the output parameters from the first inversion as the basis for the next solution and so on, effectively converging to the final output. Noisy data were also suppressed, or weighted less in the solution, to speed up convergence and improve L2-norm. The combination of data filtering and inversion techniques often reduced the RMSE to 5% which is satisfactory for such rocky heterogeneous terrain. Finally, we conducted an error analysis to strengthen the validity of our conclusions, which is presented in the Results.

2.4. Results

2.4.1. Synoptic Surveys (without Artificial Rainfall)

We first interpret subsurface geology via individual resistivity tomograms taken in dry conditions. These tomograms show areas of low and high resistivity, which are interpreted as geologic structure. We associate low resistivity regions (blue) with finely crushed material (small rock fragments and rock particles with soil-like texture) and high resistivity materials (red) with either bedrock, or large boulders and void spaces (Anterrieu et al., 2010). Small rock fragments retain water better than bedrock, boulders, or void spaces, contributing to the lower resistivity of the former.

The upper portion of the longitudinal survey of the fill (top 15-25 m in the center of the longitudinal transect, Figure 2-5a) consists of lower resistivity material (blue), while the lower portion (25-75 m deep in the center) has highly resistive portions (red-orange). This indicates that there are two main structural layers in the valley fill; the upper more closely resembles soil, although comprised of rock fragments, while the lower is likely composed of large boulders and voids. The transverse survey, taken at longitudinal meter marker 40, does not image as deep due to the topography of the transect, but does suggest that the upper portion of the fill has a lower resistivity (meters 60-130, Figure 2-5b) than the adjacent natural slopes (meters 0-60 and 130-190). From position 0 to 20 m a natural bedrock shelf exists (red) with moisture trapped above it (blue). This was confirmed by saturated soil conditions on site. Also, from position 50-60 m and 125-135 m the two side drains become evident. These features are constructed of boulders with large voids for stormwater to flow through, which were visible from the surface. In the tomogram, the side drains appear as highly heterogeneous signatures at the surface with a conductive (blue) zone directly below the land surface. Electrode installation was difficult at the position of the drains, so this high variability is expected.

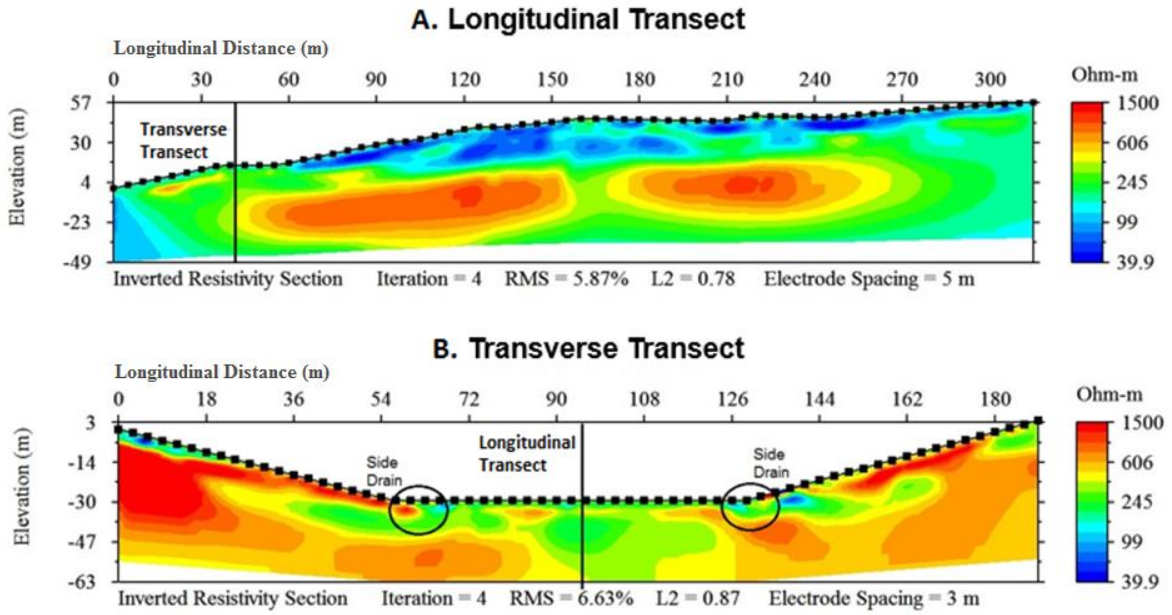

Figure 2-5. Longitudinal and transverse tomograms of valley fill. These large scale individual resistivity tomograms show electrical resistivity (Ohm-m) where areas of greater resistivity are red. They are acquired in dry conditions and show the general subsurface structure of the fill, slopes outside of the side drains in transverse transect are natural. Elevation (y-axis) is relative. (Longitudinal taken on July 31, 2014 and Transverse taken on May 22, 2014).

Control (dry condition) surveys were also acquired before the onset of artificial rainfall experiments. A pattern of intermingled high and low resistive zones emerges at each scale (Figure 2-6). Interestingly, this pattern is seemingly independent of transect length, indicating that heterogeneity exists within the valley fill at multiple spatial scales. For example, the 300 m transect (Figure 2-6a) shows the overall depth of penetration of fine-grained materials and hence water into the valley fill interior (blue regions, top 15-25 m), while the 32 m transect (Figure 2-6c) shows soil development and associated water ponding at the very shallowest depths (blue, top 1-2 m). Also, as a measure of consistency, the same geologic features are evident at each scale. Figure 2-6b is outlined in black in Figure 2-6a, and Figure 2-6c is outlined in black in Figure 2-6b. Figures 2-6b and 2-6c appear similar to the boxed region in the panel immediately above each, but with higher resolution.

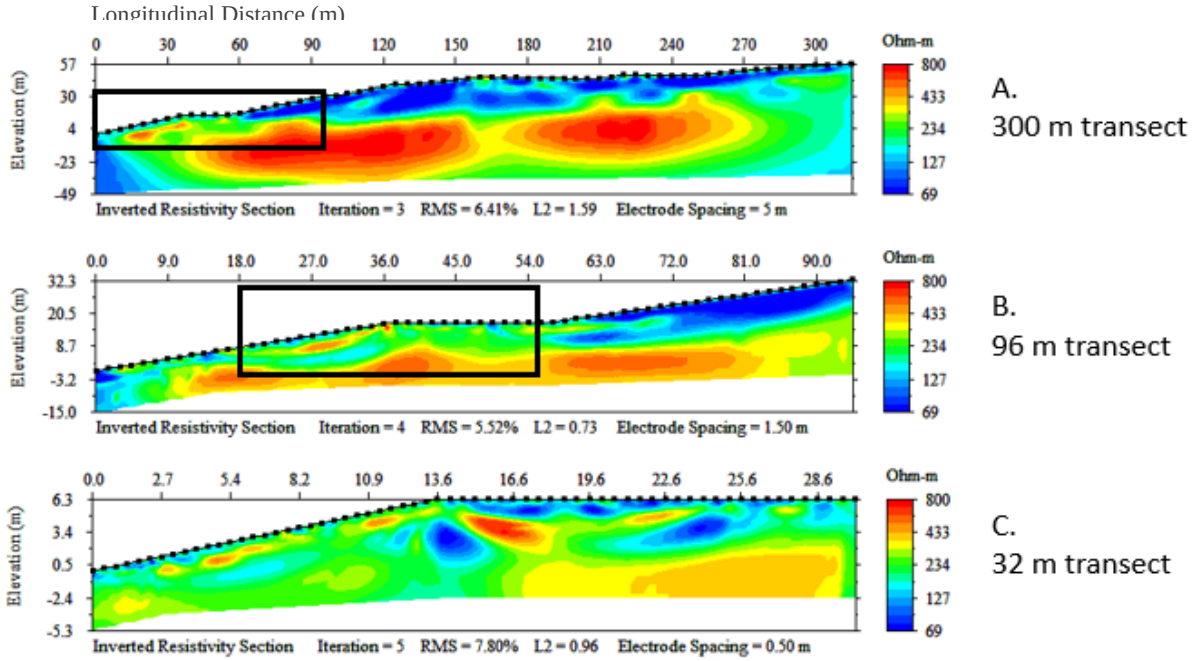

Figure 2-6. Tomograms showing subsurface heterogeneity at various scales. Individual resistivity tomograms taken in dry conditions showing electrical resistivity (Ohm-m) where areas of greater resistivity are red. Similar patterns of heterogeneity seen at different transect lengths, indicate that ERI picks up multiple scales of heterogeneity. Black box in panels A and B outline the extent of the panel immediately beneath (B and C, respectively). (A: July 31, 2014, B: July 17, 2014, C: July 31, 2014).

2.4.2. Artificial Rainfall Experiments

The artificial rainfall experiments combined with many ERI surveys taken at different times and electrode intervals reveals valley fill stormflow hydrology. Each of the experiments was conducted on different days, under somewhat varying antecedent moisture conditions (Table 2-1), and the electrodes were moved each time. Thus, results from different experiments are not directly comparable, but rather themes may be carried from one experiment to the next.

(i) Time-lapse Tomograms – Dry Antecedent Conditions

This section presents time-lapse tomograms, which do not contain information regarding the subsurface structure, but rather reveal changes through time. Only increasing electrical conductivity (yellow-orange) and decreasing electrical conductivity (blue) are shown (e.g. Figure 2-7, 2-8). These differences are then interpreted to be either transmissive zones that are becoming saturated with electrically conductive water (yellow-orange), or as areas that do not allow as much infiltration of water such as compacted layers or void spaces (blue). Assuming that there is no change in soil the structure over the time of the experiments, an increase in water saturation is the only way to induce a change in electrical conductivity response (Travelletti et al., 2012) as an increase electrical conductivity (red areas). As a result, any decrease in electrical conductivity (increase in resistance, blue) in the tomograms is not a physically possible response

to adding water to the system. Rather, it is the way the earth meter indicates that it is detecting the increased contrast between a layer that has increased electrical conductivity and an immediately adjacent layer that has remained the same (note that the blue areas are all adjacent to red areas rather than occurring as outliers). Blue and green areas are both interpreted as no change. A 10-20% change in electrical conductivity has previously been considered sufficient to indicate hydraulic change (Travelletti, 2012; Menichino, 2014), so we adopt the same threshold here.

We start with the longest transect (least spatial resolution) (RN41-RN45), with electrodes placed every 1.5 meters over a distance of 96 meters (Table 2-1). Among the experiments with dry antecedent conditions, this experiment had the longest rainfall duration at a total of 5 hours. We were able to visualize both infiltration and development of preferential flow paths. Figure 2-7a shows that after 1:15 of the rainfall event, the presence of water has started to increase the electrical conductivity at the surface (red). Some infiltration has also occurred below the rainfall plot, at meter 45, at -10 meters depth (yellow) as well as between 30 and 39 m, and at a depth of -20 m (yellow). After a time of 2:30, the infiltrated water between 30 and 39 m has become more pronounced (yellow became orange). After 5 hours even more water has infiltrated below the surface (thickening of the red region), as well as more infiltration at depth (large yellow-orange area between 40 and 60 m, and a depth of -15 m). Finally, these time-lapse tomograms reveal the inundation (or delayed saturation of) of a lateral preferential flow path to the lower left (downslope) of the rainfall plot. At time 1:15 this is shown only as a small yellow region at 35 m and -5 m depth; at time 5:00 (Figure 2-7d) this is shown as a long yellow streak from 23 to 35 m at a depth of -5 m. By contrast, the blue areas (e.g., 38 m and 53 m at -5 m depth) are likely compacted areas where conductive water does not infiltrate (Anterrieu et al., 2010). This type of lateral preferential flowpath in valley fills is consistent with previous studies (Hawkins and Aljoe, 1992; Wunsh et al., 1999).

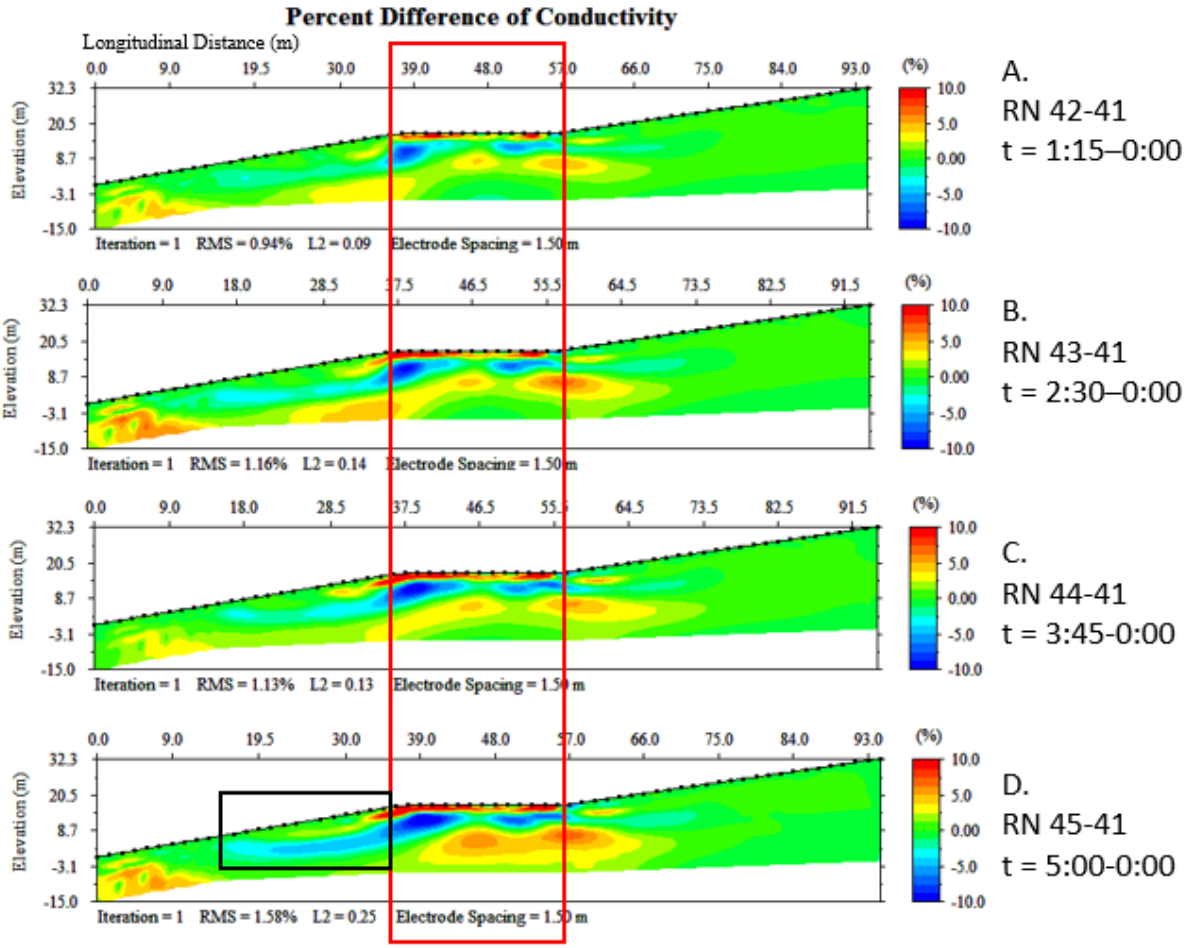

Figure 2-7. Time-lapse tomograms of artificial rainfall experiment with 1.5 meter spacing, RN4X. Time-lapse tomograms showing percent change in electrical conductivity (%) where areas of increased electrical conductivity (water content) are red, and inversion artifacts are blue. Notice that infiltration of conductive rainwater has already begun at 1:15, and continues up to 5:00 with some preferential flow developing within the black box. Red box indicates location of rainfall plot (area where artificial rainfall was applied). July 17, 2014.

In another experiment (RN52-RN55) we focused on the area of interest below the rainfall plot with a shorter transect length to allow for higher spatial resolution (Table 2-1). The experiment used an electrode spacing of 0.5 m (32 m transect) (Figure 2-8). After 45 minutes into the rainfall event (Figure 2-8a) the surface had wetted (red between 18 and 29 m, -1 m depth) and some infiltration occurred between 13 and 15 m at -10 meters depth (yellow). The surface becomes more and more conductive through time (wet/red), with most of the water staying within one meter of the surface. Increases in electrical conductivity (degree of saturation) are observed between 13 and 15 m at a depth of -10 m at times 1:30 and 2:15 (yellow became orange). Finally at time 2:15 infiltration occurs between 24 and 27 m at a depth of -5 m (orange) possibly due to the delayed activation of a preferential flow path.

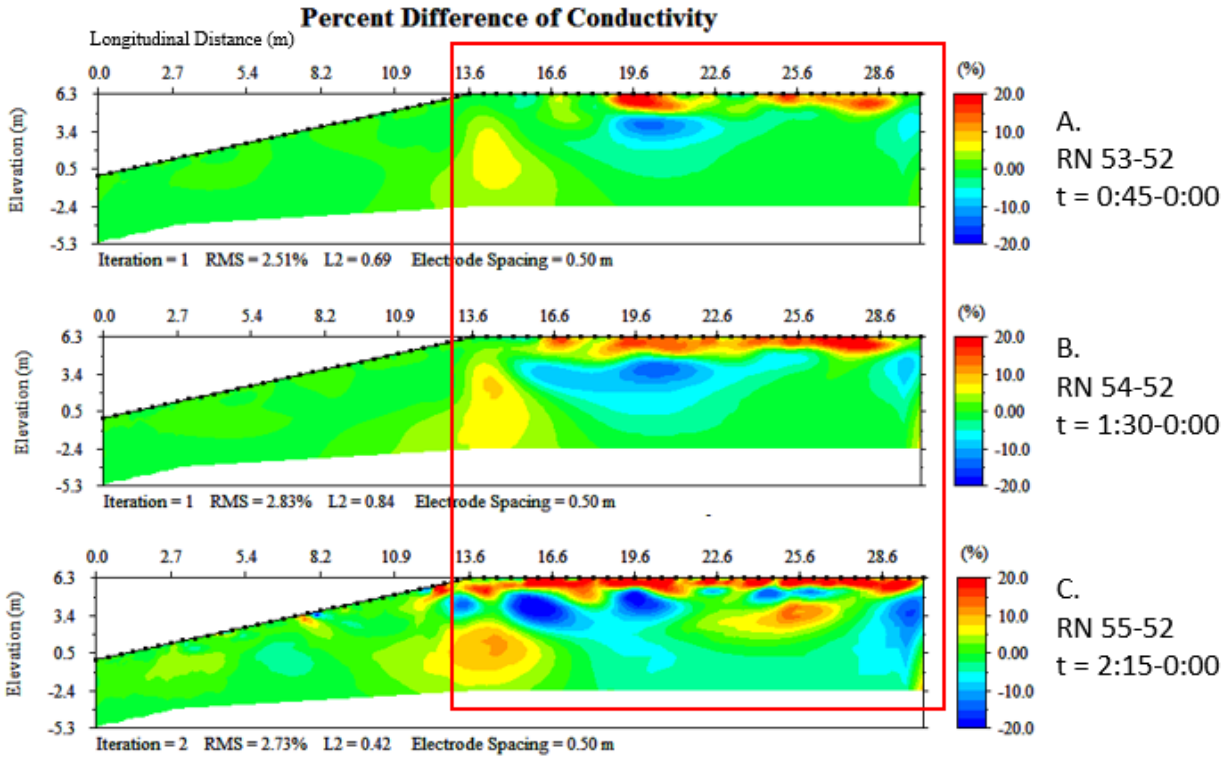

Figure 2-8. Time-lapse tomograms of artificial rainfall experiment with 0.5 meter spacing, RN5X. Time-lapse tomograms showing percent change in electrical conductivity (%) where areas of increased electrical conductivity (water content) are red, and inversion artifacts are blue. These tomograms are shallow enough to reveal saturated conditions at the surface and infiltration beneath 15 and 25 m. July 31, 2014. Red box indicates location of rainfall plot.

(ii) Time-lapse Tomograms – Wet Antecedent Conditions

In order to contrast with the dry antecedent condition time lapse tomograms (Figures 2-7, 2-8), a wet antecedent rainfall experiment was also conducted (RN31-RN34) (Figure 2-9) in which the soil profile had drained for only 16 hours since the end of a previous rainfall experiment. The electrode spacing was 1 m, for a transect length of 64 m. After 45 minutes into the rainfall experiment (Figure 2-9a) the surface had become somewhat more conductive (red), with another increase in electrical conductivity at 40 m and at a depth of -15 m. At time 2:15 (Figure 2-9c), the surface had become even more conductive and the near surface flowpath to the lower left of the image is developing more conductive regions (small yellow regions from 17-30 m at -3 m depth). The brief drain time since the previous artificial rainfall likely allowed only the largest pores to drain with the small pores remaining saturated, indicating that the residence time of infiltrated water in the spoil is often longer than 16 hours.

One of the values of the wet conditions survey is that it may reveal how infiltrating water picks up TDS, in addition to movement of the water itself. Since the control survey was taken in wet conditions, we can conclude that any differences between tomograms would show a wet to

saturated transition with downward water movement, rather than a dry to wet transition. Therefore, we wondered if it would be possible to visualize the accumulation TDS by the increase in electrical conductivity being greatest at depth. A slight increase in electrical conductivity occurs at depth (40 m, -15 m depth), however this occurrence does not increase with time. Therefore we assume that this is the inundation of a preferential flow path that has drained in the 16 hours prior, and that the effect of the fill adding TDS to the water is not visualized by ERI. This is likely due to 1) preferential flow paths are likely already leached of TDS causing salts (Parker, 2013) 2) the infiltrated water was highly conductive, so any further increases result in minimal percent change in electrical conductivity and 3) the change caused by increasing water content is larger than the change caused by increasing the electrical conductivity of the water.

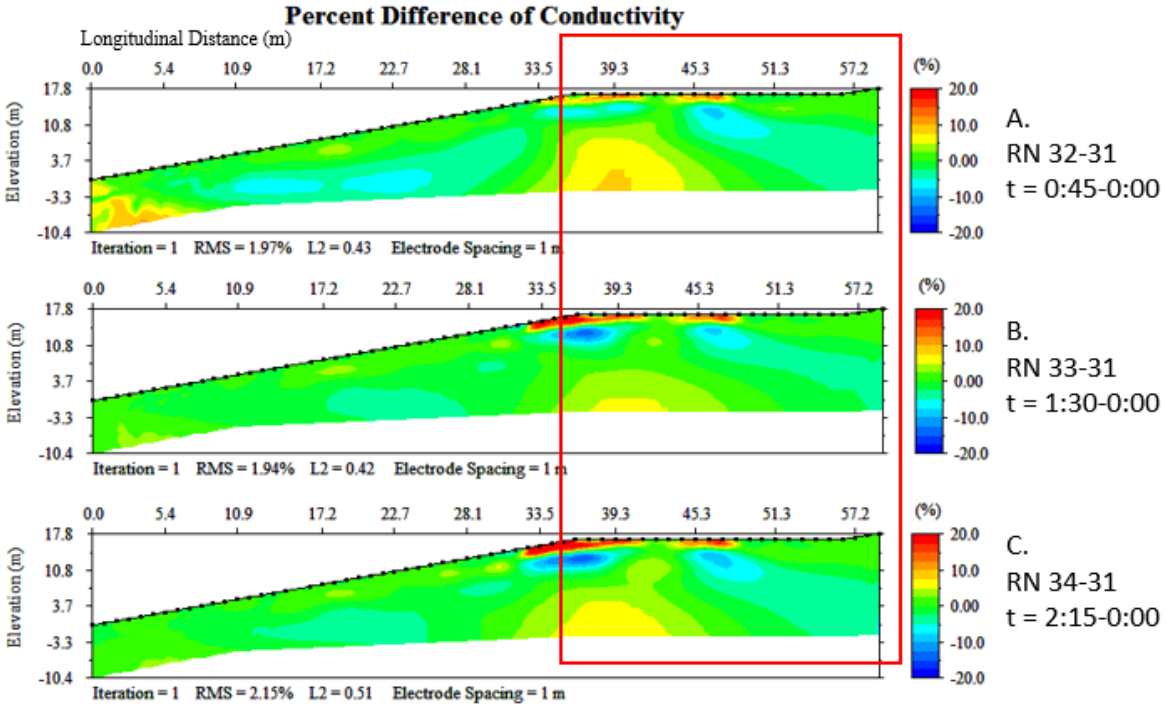

Figure 2-9. Time-lapse tomograms of artificial rainfall experiment with 1.0 meter spacing, RN3X. Time-lapse tomograms showing percent change in electrical conductivity (%) where areas of increased electrical conductivity (water content) are red, and inversion artifacts are blue. Some infiltration has occurred at 45 minutes, however continual increase in conductivity at depth not visualized. July 11, 2014. Red box indicates location of rainfall plot.

2.4.3. Comparison to Other Land-forms

We found that each of the three surveyed landscapes has a unique subsurface structure, based on its construction method. The valley fill profile (Figure 2-10a), described previously, has upper layers consisting of a soil-like low-resistivity matrix and a highly heterogeneous lower portion consisting of highly resistive boulders and large void spaces. By contrast, the highwall tomogram reveals an upper layer consisting of larger rocks and void spaces between 40 - 60 m, and 75 -

110 m (shown as red in figure 2-10b), which was confirmed visually on site. Below these large rocks is likely the location of the highwall, somewhere between 90 and 100 m; however this is not seen in the tomogram because coarse material at the surface prevented quality electrode installation and thus most of that data were removed during filtering. The filled portion, between 10 and 75 m has similar resistive material as the upper layer of the valley fill.

The structure of the natural slope is much more homogeneous than the other land-forms. The surface consists of a layer of spongey woody debris and weathered rock which is imaged as being highly resistive due to a lack of conducive salts in the pore water (Figure 2-10c). The subsurface consists of consolidated bedrock which is generally more resistive than the fine near-surface material in the valley fill. There are natural variations in the resistivity of this bedrock represented as smooth transitions among resistance values; however none of the variations are as drastic as those of the filled slopes. It is worth noting that the natural slope survey was conducted in colder temperatures than the others, which can cause a slight increase in resistance in the top 0.5 – 1.0 meter (Tavelletti et al., 2012). Variability due to temperature differences is addressed in the Error Analysis.

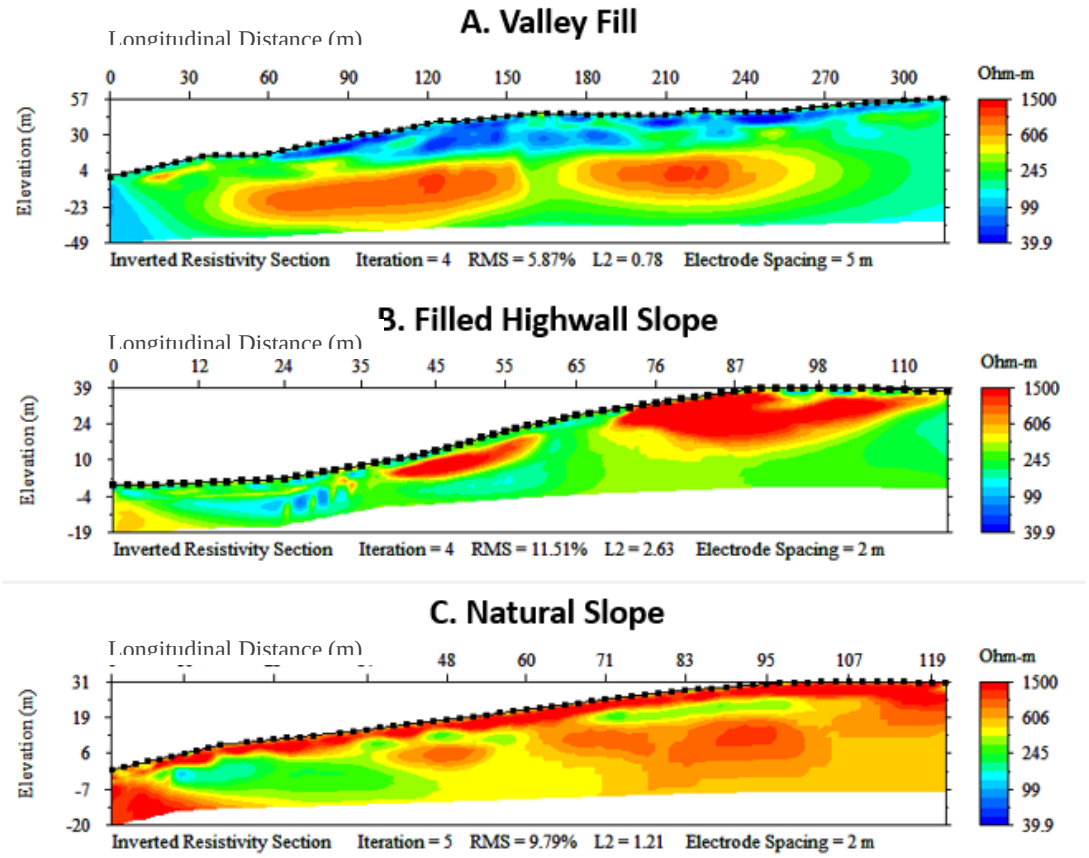

Figure 2-10. Tomograms of three different landscapes. Individual resistivity tomograms showing electrical resistivity (Ohm-m) where areas of greater electrical resistance is red. Structural differences between the three types of landscapes were captured in the ERI surveys. Note differences in transect length (natural slope and highwall transects are shorter than valley fill transect). (A: July 31, 2014, B: August 13, 2014, C: November 15, 2014)

2.4.4 Error Analysis

(i) Error Extent and Location

We conducted a qualitative error analysis to evaluate the impact of method limitations on the study conclusions. RMS and L2-norm values were provided in each tomogram (Figures 2-5 through 2-10), and are summarized in Table 2-2. These values quantify how error varies within and among the different experiments/surveys. Generally, the time-lapse tomograms have much lower RMS and L2-norm than the individual resistivity inversion tomograms, as is expected because systematic errors are removed (discussed in Methods). Also, the surveys with the worst electrode-earth connection have the highest errors (Filled Highwall Slope and Natural Slope) because a substantial amount of the data was filtered out.

Table 2-2. Summary of RMS and L2-norm errors. This table summarizes the calculated error factors for each survey. Notice that the time lapse inversion tomograms have lower RMS and L2-norm than the individual resistivity inversion tomograms. Surveys with the worst electrode-earth connection have the highest errors (Filled Highwall Slope and Natural Slope).

Survey	**Figure**	**RMS**	**L2-norm**
Longitudinal	2-5a, 2-6a, 2-10a	5.87-6.41	0.78-1.59
Transverse	2-5b	6.63	0.78
RN41	2-6b,	5.52	0.73
RN52	2-6c	7.80	0.96
RN42-41 to RN45-41	2-7, a-d	0.94-1.58	0.09-0.25
RN53-52 to RN55-52	2-8, a-c	2.51-2.83	0.42-0.84
RN32-31 to RN34-31	2-9, a-c	1.94-2.15	0.42-0.51
Filled Highwall Slope	2-10b	11.51	2.63
Natural Slope	2-10c	9.79	1.21

Here we add Data Misfit Pseudosections created by EarthImager to provide a visual representation of how and where error was induced. For a majority of the tomograms (Figures 2-5 - 10), the error remaining after data filtering and inversion was either isolated at the surface (uppermost 2 meters) and caused by imprecision in measurement by the earth meter (observational noise) (Kemna et al., 2002), or begin at the surface and extend deep into the subsurface (Figure 2-11) and caused by missing data lost during filtering due to poor electrode-earth connection. In Figure 2-11, black dots represent data points, and colored areas without black dots are areas that have had data filtered out. Due to the large amount of missing data there are erroneous regions in the tomogram (post-inversion) where the data still do not fit the solution, these regions may be more (red) or less (blue) resistive than the inverted solution proposes.

Errors induced by observational noise in the surface as well as by missing data likely have a negative impact on the resolution of a few of the tomograms, but do not impact our conclusions. Observational noise does not affect results as only basic conclusions were drawn in the near-surface zone (increasing electrical conductivity with rainfall) and in the tomograms most

important for near-surface conclusions (RN3X, Figure 2-9b, c) there was no visible error remaining at the surface of the pseudosections. Missing data appear in the individual resistivity inversion tomograms as areas of low resolution, and knowing where they are via the Relative Data Misfit Pseudosections allowed us to not draw conclusions on those areas; for example, the data missing in the upper right of Figure 2-11 is represented in Figure 2-10b as the large resistive (red) region between meters 75 and 110. In time-lapse tomograms areas that have data filtered out do not appear to change through time, so false conclusions are not drawn in those areas either. Therefore, while observational noise and missing data induced errors are important to consider, they do not strongly impact the study conclusions.

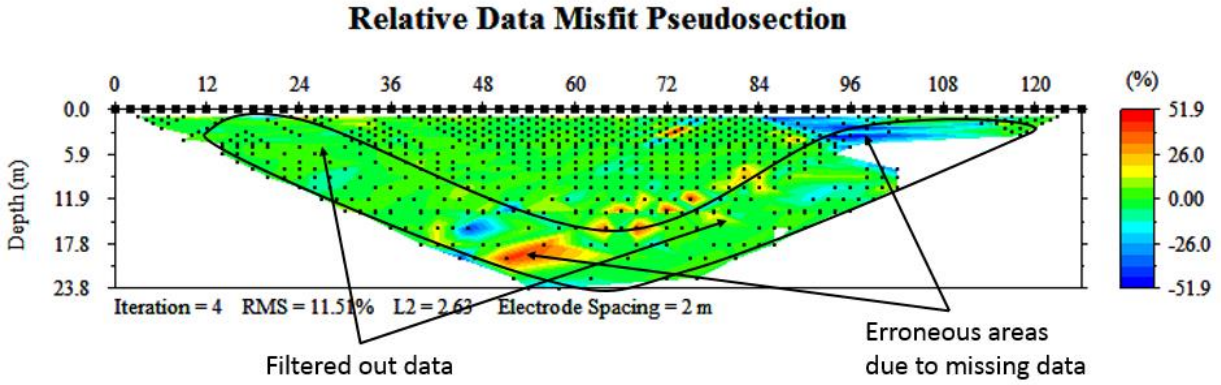

Figure 2-11. Relative Data Misfit Pseudosection of Filled Highwall Slope. Post-inversion data misfit is represented by red and blue regions, and caused by the absence of data points due to filtering in those areas. This is the Filled Highwall Slope, and missing data in the upper right in this figure is represented in Figure 2-10b simply as a highly resistive (red) region.

(ii) Temperature Induced Error

Temperature is another possible source of error in ERI studies. Resistivity is a temperature dependent material property (Campbell et al., 1948; Keller, 1987), thus a variety of ERI studies have done an adjustment to account for error induced by temperature variation in the soil profile (Brunet et al., 2010; Coscia et al., 2012; Travelletti et al., 2012). Yet others have neglected temperature entirely (Seaton and Burbey, 2002, Ward et al., 2010; de Bari et al., 2011; Meyerhoff et al., 2014). Similarly, temperature has been also been disregarded on the basis that the investigated medium did not deviate by more than 1˚C over the course of the 90 day study (Kemna et al., 2002). In the analysis presented above, temperature was neither measured nor calibrated for because previous studies have found that the impact of temperature on resistivity values is negligible at depths greater than a half a meter (Brunet et al., 2010; Travelletti et al., 2012); and because the uppermost half meter of the results likely have noise and missing data induced errors that exceed temperature related errors.

2.5 Discussion

2.5.1 Valley Fill Hydrology

Our results provide a better understanding of the subsurface structure and hydrologic regime of valley fills. In regards to structure, our synoptic tomograms of the valley fill confirm that the upper layers are largely composed of small compacted rock fragments with increasing boulder size and void space with depth (Chong and Cowsert, 1987; Potter et al., 1988; Guebert and Gardner, 2001; Miller and Zegre, 2014). Heterogeneities occur within each layer (upper and lower), for example the upper layer may contain rocks ranging from 0.01 m to 0.5 m in diameter, while the lower layer may have boulders ranging from 0.5 m to 3.0 m in diameter. This is consistent with Anterrieu et al. (2010) who found a similar pattern of heterogeneity at different scales in mine spoil.

In regards to hydrology, it is apparent that a large amount of stormwater either accumulates on the surface above a compacted layer, or infiltrates deeply and quickly along preferential flow paths. Our results indicate that widespread infiltration into the matrix (i.e. the wetting front) remains quite shallow (1 meter) even after 2:15 hours of heavy rainfall. In addition to matrix infiltration, there is also preferential flow through the compacted layer. Of these preferential flow paths, some are horizontal, possibly created by various degrees of compaction along angle-of-repose surfaces, while others are vertical and quite deep. Our results indicate that water can reach a depth of up to 10 meters in 45 minutes. During a storm event there is likely a significant amount of overland flow, with infiltrating water moving quickly along preferential flow paths, which is consistent with previous studies (Guebert and Gardner, 2001; Miller and Zegre, 2014). Mine spoil stormwater flow paths indeed resemble pseudokarst, with many complicated flowpaths and patterns (Caruccio and Geidel, 1984). These preferential flow paths have also been referred to as snakeholes (Wunsch et al., 1999). The points along the surface and in the subsurface at which the water changes routes or directions have been recently referred to as control points (Evans et al., 2015).

Such preferential flow also means that significant portions of the subsurface of this fill may not typically experience much infiltrating stormwater. Our results also indicate that stormwater infiltration may be limited in its contribution to high TDS in the effluent stream because the combination of low infiltration capacity and preferential flow would greatly decrease the surface volume of fill material exposed to stormwater. Preferential flow is rapid and thus decreases the time of saturation in which TDS would be acquired and is along fairly stable flowpaths which are already leached. Groundwater moving slowly and deeply from upslope mining areas through the valley fill therefore may be an additional source of TDS. This is an important area for future research.

2.5.2 Method Development and Limitations

(i) Method Development

Preferential flowpaths in valley fills have previously been assumed (Caruccio and Geidel, 1984; Wunsh et al., 1999; Miller and Zegre, 2014) and inferred from groundwater slug tests (Hawkins 2004) but never before been visualized directly. Valley fills are a challenging setting for hydrologic investigation because the rocky soils and subsurface prevent easy installation of

piezometers or groundwater wells, the use of infiltrometers, and unnatural subsurface may complicate tracer studies. Therefore, less invasive tools are required. While ERI has been applied to long term spoil monitoring (Wangerud et al., 2006) as well as a mine-spoil structure investigation (Anterrieu et al., 2010), these studies do not generate refined spatial-temporal relationships such as the inundation of preferential flow paths which we have captured here. By using ERI, we have successfully increased the scope of hydrologic investigation techniques available in a mine spoil environment.

(ii) Study Limitations

ERI does not detect water presence directly, rather it is through interpreting regions of low and high resistance that hydrologic conclusions are drawn. When representing dynamic processes, conclusions are not meant to be drawn on absolute resistivity value, rather we primarily rely on time-lapse inversions (Kemna et al., 2002; Samouëlian et al., 2005). Because tomograms are a modeled solution to an ill-posed (i.e. non-unique solutions exist) and ill-conditioned (i.e. small error in the data may lead to large error in the solution) problem (AGI, 2009, Menichino et al., 2014), absolute resistivity values and exact locations are subject to greater uncertainty than spatial trends. ERI is an advancement over traditional hydrologic investigation techniques because errors induced by the earth meter and inversion process as well as the increasing uncertainty at depth are less significant than that which is induced via interpolation between point measurements (Crook et al., 2008). The hydrologic interpretation used here has been shown as viable by previous studies (Travelletti et al., 2012; Menichino et al., 2014).

Temporal resolution was another study limitation. The chosen array, number of electrodes, and earth meter used for this study resulted in data collection time for a single survey of 35 minutes. Faster data collection with more frequent surveys may have revealed more about the wetting-up process and preferential flow path inundation. More frequent surveying in the beginning of each dry condition rainfall experiment would have resulted in more incremental variation between subsequent time-lapse tomograms, rather than just showing considerable change between the control and the first monitor survey (i.e. Figure 2-7a). We recommend that future studies use a shorter time interval for surveys at the beginning of an artificial rainfall experiment, and a longer time interval late in an experiment in order to capture quickly occurring changes initially while extending the results for longer precipitation events. Yet we note that more frequent tomograms would require fewer electrodes in the transect, which necessarily reduces the spatial resolution of the tomograms. This tradeoff between spatial and temporal resolution is fundamental to ERI.

Installation of electrodes in mine spoil was another study limitation. Some, but not all regions into which electrodes were installed consist of primarily medium to large sized rocks (ex. Figure 2-10b, meters 75-110). Despite making small scale adjustments to electrode location in preference of finer textured soil material, pouring water on the electrodes, and conducting multiple resistance tests, some electrodes were never installed well enough to collect data that was not lost during filtering. Results would have been more detailed and possibly conveyed more information had these electrodes collected reliable data. While this rocky surface material is inherent in mined landscapes, it was left largely uncontrolled due to the large number of transects used in this study. Future studies could possibly benefit from more invasive electrode installation

methods such as digging up a small cylinder where the electrode is to be installed and packing it with bentonite.

2.5.3 Applied Value

ERI may have beneficial applications for the mining industry and surrounding communities. It could be used to study how geologic structural variation among valley fills with different construction techniques, reclamation techniques, and age influence effluent stream water quality. Previous models have forecasted that an alternative valley fill design, known as geomorphic design, could decrease effluent water contamination (DePriest, 2012). If ERI was used in conjunction with traditional water quality analyses the model results could be field tested. If these studies were repeated on multiple valley fill construction types the way in which design impacts hydrology could be determined.

Our data show the majority of the volume of the valley fill likely experiences little infiltrated stormwater because most of it is routed to narrow preferential flowpaths, and thus stormwater may not be the primary source of TDS. This knowledge could lead to the design of valley fills in ways that limit weathering where TDS contributions are most significant. For example, if the main source of TDS was groundwater moving through the fill (rather than stormflow), then a valley fill design that has inert conduits (e.g. concrete or rock channels constructed with durable and low-TDS generating rock materials, such as siliceous sandstones) at depth could decrease weathering and TDS-generation effects. ERI could then monitor not only water infiltrating the valley fill from the surface, but also upgradient groundwater from the mine itself moving through the fill and possible conduits. Without ERI, differences in flowpaths that result from various construction methods must be assumed, rather than visualized.

Our results also indicate that there is minimal opportunity to retrofit existing valley fills to reduce TDS output. Due to preferential flow and compaction decreasing the surface area for weathering, TDS may also be generated in groundwater flowing beneath the fill. Thus blocking infiltration along preferential flow paths with bentonite or clay caps will not likely decrease TDS. Further, noting that groundwater generally begins in upland mine spoil piles, it may important to control and reduce TDS generation at the upland source, rather than solely in the valley fill. Options to consider here would be an impermeable membrane beneath the spoil pile but above the water table, or around the periphery. Such solutions would require construction costs and maintenance, so the consequences would need to be evaluated holistically.

2.6 Conclusions

We have shown that ERI can be successfully applied on valley fills to image both subsurface structure and water movement where traditional hydrologic methods are difficult to employ. The tomograms reveal that the upper portion (top 15-25 meters) of the valley fill is composed of finer material and the lower portions are composed of larger rocks with many void spaces (deeper 25-75 m) (Figure 2-5a). Tomograms allowed us to visualize the high degree of variability of the fill when compared to adjacent natural slopes (Figure 2-5b) and capture the effect of side drains (meters 50-60 and 125-135, Figure 2-5b). There is overall a high level of geologic heterogeneity, and such heterogeneity exists at multiple scales within the fill (black boxes, Figure 2-6).

Compacted fines at the surface of the valley fill led to water ponding, substantial surface runoff, and minimal infiltration into the soil-like matrix. Water that did infiltrate the surface layer did so quickly through preferential flowpaths. Infiltrated water was then either forced to flow laterally in relatively shallow preferential flowpaths within the compacted layer (black box, Figure 2-7d) or it infiltrated vertically to substantial depths within the fill. For example, we observed water moving from the surface down to a depth of 20 m in as little as 1:15 hours (Figure 2-7a) and to a depth of 10 m in just 45 minutes (Figure 2-8a).

The ability of ERI to detect variations in subsurface structure was confirmed by synoptic surveys of two other sites with contrasting history. A tomogram from a filled highwall slope showed very rocky regions in shallower locations than they were in the valley fills (meters 46-60 and 75-110, Figure 2-10b). While the rest of the fill had high spatial heterogeneity, similar to the valley fill. By contrast, a tomogram from a natural (unmined) slope showed lower overall spatial heterogeneity, consistent with undisturbed bedrock (Figure 2-10c). The weathered rock was imaged as a highly resistive surface layer (uppermost 5 meters, Figure 2-10c).

These geologic and hydrologic insights demonstrate ERI's potential for revealing subsurface structural characteristics within what was formerly viewed as a "black box" in the interior of valleys fills and mined landscapes. ERI is well suited for this application because it is non-invasive, is capable of monitoring spatiotemporal changes, and can yield a cohesive subsurface map rather than simply point measurements with interpolation. ERI can be used in the future to monitor preferential flow in mine spoil of other construction methods, such as the geomorphic valley fill, to determine how fill construction methods impact downstream water quality. This knowledge in turn could allow development of improved valley fill or upland spoil pile construction techniques. Steady refinement of construction methods could eventually result in the valley fill that does not experience the typical hydrologic effects of MRM /VF operations. By adjusting the hydrology of the valley fill, it is conceivable that water quality issues, most specifically elevated TDS, could be reduced and the impact they have on ACR ecology ameliorated.

2.7 Acknowledgements

We would like to thank Wells Fargo for funding this study through the Clean Technology and Innovation Grant (views expressed in this document are those of the authors, and not necessarily those of Wells Fargo). We would like to thank all collaborators at the mine site for their support. We would like to thank all of the field assistants throughout the project including: Elyse Clark, S.M. Masud Rana, Abenezer Nida, Emily Baer, Chris Driscoll, and Ian Goodwin.

2.8 References

AGI, (2009). Instruction Manual for EarthImager 2D Version 2.4.0 Resistivity and IP Inversion Software. Advanced Geosciences, Inc. Austin, TX, USA.

Anterrieu, O., M. Chouteau, and M. Aubertin (2010), Geophysical characterization of the large-scale internal structure of a waste rock pile from a hard rock mine, *Bulletin of Engineering Geology and the Environment, 69,* 533-548, doi:10.1007/s10064-010-0264-4.

Bernhardt E.S., B.D. Lutz, R.S. King, J.P. Fay, C.E. Carter, A.M. Helton, D. Campagna, and J. Amos (2012), How many mountains can we mine? Assessing the regional degradation of central Appalachian rivers by surface coal mining. Environmental Science and Technology 46:8115-8122.

Bernhardt, E. S., and M.A. Palmer (2011), The environmental costs of mountaintop mining valley fill operations for aquatic ecosystems of the Central Appalachians, *Ann. N.Y. Acad. Sci. 1223,* 39–57, doi:10.1111/j.1749-6632.2011.05986.x.

Brunet, P., R. Clément, and C. Bouvier (2010), Monitoring soil water content and deficit using Electrical Resistivity Tomography (ERT) – A case study in the Cevennes area, France, *J. Hydrol., 380*(1–2), 146–153, doi:10.1016/j.jhydrol.2009.10.032.

Campbell R. B., C. A. Bower, and L. A. Richards (1948), Change of electrical conductivity with temperature and the relation of osmotic pressure to electrical conductivity and ion concentration for soil extracts, *Soil Sci. Soc. Am. J., 13*(C), 66–69, doi:10.2136/sssaj1949.036159950013000C0010x.

Caruccio, F. T., and G. Geidel, (1984), Induced alkaline recharge zones to mitigate acidic seeps, Proceedings of the Symposium on Surface Mining, Hydrology, Sedimentology, and Reclamation, Lexington KY, *University of Kentucky*.

Chong, S. K., and P. T. Cowsert, (1997), Infiltration in reclaimed mined land ameliorated with deep tillage treatments. *Soil Tillage Res., 44*, 255–264.

Cormier, S. M., G. W. Suter, and L. Zheng (2013a), Derivation of a benchmark for freshwater ionic strength. *Environ. Toxicol. Chem. 32*(2), 263-271, doi:10.1002/etc.2064.

Cormier, S. M., S. P. Wilkes, and L. Zheng (2013b), Relationship of land use and elevated ionic strength in Appalachian watersheds, *Environ. Toxicol. Chem., 32*(2), 296–303, doi:10.1002/etc.2055.

Coscia, I., N. Linde, S. Greenhalgh, T. Gunther, and A. Green (2012), A filtering method to correct time-lapse 3D ERT data and improve imaging of natural aquifer dynamics, *J. Appl. Geophys.80,* 12–24, doi:10.1016/j.jappgeo.2011.12.015.

Crook N., A. Binley, R. Knight, D. A. Robinson, J. Zarnetske, and R. Haggerty (2008), Electrical resistivity imaging of the architecture of substream sediments, *Water Resources Research, 44,* 1-11.

Dahlin, T., and B. Zhou (2004), A numerical comparison of 2D resistivity imaging with 10 electrode arrays, *Geophys. Prospect. 52*, 379–398.

Daily, W.D., A. L. Ramirez, D. J. LaBrecque, and W. Barber (1995), Electrical resistance tomography experiments at the Oregon Graduate Institute, *J. Appl. Geophys. 33*, 227–237.

de Bari, C., V. Lapenna, A. Perrone, C. Puglisi, and F. Sdao (2011), Digital photogrammetric analysis and electrical resistivity tomography for investigating the Picerno Landslide (Basilicata Region, Southern Italy), *Geomorphology*, *133*, 34-46, doi:10.1016/j.geomorph.2011.06.013.

DePriest, N. C. (2012) Comparison of groundwater seepage modeling in approximate original contous and geomorphic valley fill design (Master's Thesis), West Wirginia University, Morgantown WV.

Evans, D. M., C. E. Zipper, E. T. Hester, and S. H. Schoenholtz (2015), Hydrologic effects of surface coal mining in Appalachia (USA). *J. Am. Water Resour. As.* (in press).

Evans, D. M., C. E. Zipper, P. F. Donovan, and W. L. Daniels (2014), Long-term trends of specific conductance in waters discharged by coal-mine valley fills in central Appalachia, USA, *J. Am. Water Resour. As., 50(6),* 1449–1460, doi: 10.1111/jawr.12198.

Ferrari, J. R., T. R. Lookingbill, B. McCormick, P. A. Townsend, and K. N. Eshleman (2009), Surface mining and reclamation effects on flood response of watersheds in the central Appalachian Plateau region, *Water Resour. Res.*, *45*(4), n/a–n/a, doi:10.1029/2008WR007109.

French, H. K., C. Hardbattle, A. Binley, P. Winship, and L. Jakobsen (2002), Monitoring snowmelt induces unsaturated flow and transport using electrical resistivity tomography, *J. Hydrol. 267,* 273–284.

Fritz K. M., S. Fulton, B. R. Johnson, C. D. Barton, J. D. Jack, D. A. Word, and R. A. Burke (2010), Structural and functional characteristics of natural and constructed channels draining a reclaimed mountaintop removal and valley fill coal mine, *J. N. Am. Benthol. Soc. 29*, 673-689.

Geotomo, (2013), Rapid 2D Resistivity & IP inversion using the least-squares method, Geotomo Software. Panang, Malaysia.

Green, J., M. Passmore, and H. Childers (2000), A Survey of the Condition of Streams in the Primary Region of Mountaintop Mining/Valley Fill Coal Mining, US Environmental Protection Agency: Philadelphia, PA, USA.

Griffith, M. B., S. B. Norton, L. C. Alexander, A. I. Pollard, and S. D. LeDuc (2012), The effects of mountaintop mines and valley fills on the physicochemical quality of stream ecosystems in the central Appalachians: A review, *Sci. Total Environ.*, *417–418*, 1–12, doi:10.1016/j.scitotenv.2011.12.042.

Guebert, M. D., and T. W. Gardner (2001), Macropore flow on a reclaimed surface mine: infiltration and hillslope hydrology, *Geomorphology*, *39*(3–4), 151–169, doi:10.1016/S0169-555X(00)00107-0.

Hartman, K. J., M. D. Kaller, J. W. Howell, and J. A. Sweka (2005), How much do valley fills influence headwater streams?, *Hydrobiologia 532*, 91–102.

Hawkins J. W. (1998), Hydraullic properties of surface mine spoils of the Northern Appalachian Plateau, Proceedings of the 15th National Meeting of the American Society of Mining and Reclamation, St. Louis, MO, *ASMR.*

Hawkins, J. W. (2004), Predictability of Surface Mine Spoil Hydrologic Properties in the Appalachian Plateau, *Ground Water*, *42*(1), 119–125.

Hawkins, J. W., and W.W. Aljoe, (1992), Pseudokarst groundwater hydrologic characteristics of a mine spoil aquifer, *Mine Water Environ., 11(2),* 37-52.

Herman, R. (2001), An introduction to electrical resistivity in geophysics, *Am. J. Phys. 69,* 943–952, doi: 10.1119/1.1378013.

Holl, K. D. (2002), Long-term vegetation recovery on reclaimed coal surface mines in the eastern USA, *J. Appl. Ecol. 39*, 960–970.

Johnson, B. R., A. Haas, and K. M. Fritz (2010), Use of spatially explicit physicochemical data to measure downstream impacts of headwater stream disturbance. *Water Resour. Res. 46,* W09526.

Keller, G.V. (1987), Rock and mineral properties, Electromagnetic Methods in Applied Geophysics Theory: Tulsa, OK, *Soc. Explor. Geophys., 1,* 13-51.

Kemna, A., J. Vanderborgh, B. Kulessa, and H. Vereecken (2002), Imaging and characterization of subsurface solute transport using electrical resistivity tomography (ERT) and equivalent transport models, *J. Hydrol., 267,* 125-146.

Lindberg, T. T., E. S. Bernhardt, R. Bier, A. M. Helton, R. B. Merola, A. Vengosh, and R. T. D. Giulio (2011), Cumulative impacts of mountaintop mining on an Appalachian watershed, *P. Natl. Acad. Sci. USA*, *108*(52), 20929–20934, doi:10.1073/pnas.1112381108.

McCormick, B. C., K. N. Eshleman, J. L. Griffith, and P. A. Townsend (2009), Detection of flooding responses at the river basin scale enhanced by land use change, *Water Resour. Res.*, *45*(8), n/a–n/a, doi:10.1029/2008WR007594.

Menichino, G. T., A. S. Ward, and E. T. Hester (2014), Macropores as preferential flow paths in meander bends. *Hydrol. Process., 28,* 482-495.

Merricks, T. C., D. S. Cherry, C. E. Zipper, R. Currie, and T. Valenti (2007), Coal-mine hollow fill and settling pond influences on headwater streams in southern West Virginia, USA, *Environ. Monit. Assess. 129*, 359–378.

Messinger, T. (2003), Comparison of storm response of streams in small, unmined and valley-filled watersheds, 1999 – 2001, Ballard Fork, WV, Office of Surface Mining, Reclamation, and Environmen,. Water-resources Investigation Report 02-4303.

Messinger, T., and K. S. Paybins (2003). Relations between Precipitation and Daily and Monthly Mean Flows in Gaged, Unmined and Valley-Filled Watersheds, Ballard Fork, West Virginia, 1999–2001, US Geological Survey: Charleston, WV, USA, Water-resources Investigation Report 2003-4113.

Meyerhoff, S. B., R. M. Maxwell, A. Revil, J. B. Martin, M. Karaoulis, and W. D. Graham (2014), Characterization of groundwater and surface water mixing in a semiconfined karst aquifer using time-lapse electrical resistivity tomography, *Water Resour. Res., 50,* 2566–2585, doi:10.1002/ 2013WR013991.

Miller, A. J., and N. P. Zegre (2014). Mountaintop Removal Mining and Catchment Hydrology. *Water*, *6,* 472-499. doi:10.3390/w6030472.

Morris, M., J. S. Rønning, and O. B. Lile, (1996), Geoelectric monitoring of a tracer injection experiment: modeling and interpretation, *Eur. J. Environ. Engng Geophys. 1*, 15–34.

Negley, T. L., and K. N. Eshleman (2006), Comparison of stormflow responses of surface-mined and forested watersheds in the Appalachian Mountains, USA, *Hydrol. Process.*, *20*(16), 3467–3483, doi:10.1002/hyp.6148.

Osiensky, J. L., and P. R. Donaldson (1995), Electrical flow through an aquifer for contaminant source leak detection and delineation of plume evolution, *J. Hydrol. 169*, 243–263.

Oursingbe M., T. Zhonghua, B. W. Oyelola, and Z. Mahamadou (2012), Groundwater exploration in the basement of Lake-Oro District-Chad, using electrical resistivity imaging approach, Afr. J. Pahrm. Pharmaco., 7(19), 2720-2729, doi: 10.5897/IJPS11.961.

Palmer, M. A., E. S. Bernhardt, W. H. Schlesinger, K. N. Eshleman, E. Foufoula-Georgiou, M. S. Hendryx, A. D. Lemly, G. E. Likens, O. L. Loucks, M. E. Powers, P. S. White, and P. R. Wilcock (2010), Mountaintop Mining Consequences, *Science*, *327*(5962), 148–149, doi:10.1126/science.1180543.

Parker, J. M., (2013), Effect of Various Saturation Levels, Leaching Solution pH, and Leaching Cycle on Electrical Conductivity of Coal Mine Spoil Leachate (Master's Thesis), Virginia Polytechnic and State University, Blacksburg VA, USA.

Peng, S. S. (2000), Mountaintop removal controversy slows West Virginia coal mining. *Min. Eng.*, *52*, 53–58.

Petty, J. T., J. B. Fulton, M. P. Strager, G. T. Merovich, J. M. Stiles, and P. F. Ziemkiewicz (2010), Landscape indicators and thresholds of stream ecological impairment in an intensively mined Appalachian watershed, *J. North Am. Benthol. Soc. 29*, 1292–1309.

Phillips, J. D. (2004), Impact of surface mine valley fills on headwater floods in eastern Kentucky, *Environ. Geol. 45*, 367-380, doi:10.1007/s00254-003-0883-1.

Pond, G. J., M. E. Passmore, F. A. Borsuk, L. Reynolds, and C. J. Rose (2008), Downstream effects of mountaintop coal mining: comparing biological conditions using family- and genus-level macroinvertebrate bioassessment tools, *J. N. Am. Benthol. Soc.*, *27*(3), 717–737, doi:10.1899/08-015.1.

Potter, K., F. Carter, and E. Doll (1988), Physical properties of constructed and undisturbed soils. *Soil Sci. Soc. Am. J.*, *52*, 1435–1438.

Roningen J., and T. J. Burbey (2012), Hydrologic controls on lake level: a case study at Mountain Lake, Virginia, USA, *Hydrogeol. J. 20*, 1149-1167, doi:10.1007/s10040-012-0859-x.

Rugh, D. F., and T. J. Burbey (2008), Using saline tracers to evaluate preferential recharge in fractured rocks, Floyd County, Virginia, USA, *Hydrogeol. J. 16*, 251-262, doi:10.1007/s10040-007-0236-3.

Samouëlian A., I. Cousin, A. Tabbagh, A. Bruand, and G. Richard (2005), Electrical resistivity survey in soil science: a review, *Soil & Tillage Research 83,* 173–193.

Saylor, K. L. (2008), Land Cover Trends Project: Central Applachians. U.S. Department of the Interior, U.S. Geological Survey. Washington, DC. Retrieved from: http://landcovertrends.usgs.gov/east/eco69Report.html.

Seaton, W. J., and T. J. Burbey (2002), Evaluation of two dimensional resistivity methods in fractured crystalline-rock terrane, *J. App. Geophys., 51*, 21-41.

Simmons, J., W. Currie, K. Eshleman, K. Kuers, S. Monteleone, T. Negley, B. Pohlad, and C. Thomas (2008), Forest to reclaimed land use change leads to altered ecosystem structure and function, *Ecol. Appl. 18*, 104–118, doi:10.1890/07-1117.1.

Slater, L., A. Binley, R. Vertseeg, G. Cassiani, R. Birken, and S. Sandberg (2002), A 3D ERT study of solute transport in a large experimental tank, *J. App. Geophys. 49*, 211-229.

Timpano A.J., S.H. Schoenholtz, D.J. Soucek, and C.E. Zipper (2015), Salinity as a limiting factor for biological condition in mining-influenced Central Appalachian headwater streams, Am. Wat. Res., 51, 240-250.

Travelletti, J., P. Sailhac, J. P. Malet, G. Grandjean, and J. Ponton (2012), Hydrological response of weathered clay-shale slopes: water infiltration monitoring with time-lapse electrical resistivity tomography, *Hydrol. Process.*, *26*(14), 2106–2119. doi:10.1002/hyp.7983.

U.S. Environmental Protection Agency (2011), The Effects of Mountaintop Mines and Valley Fills on Aquatic Ecosystems of the Central Appalachian Coal Fields. *EPA 600-R09-138F*, Office of Research and Development, Washington, D.C.

U.S. Geological Survey (2013) Virginia Geology, Mineral Resources On-Line Spatial Data, Retrieved from: http://mrdata.usgs.gov/sgmc/va.html.

Wangerud, K., R. Versteeg, G. Heath, R. Markiewicz, and A. Richardson (2006), Insights into hydrodynamic and geochemical processes in a valley fill ARD and waste rock repository from an autonomous multi-sensor monitoring system, Proceedings of the 7th International Conference of Acid Rock Drainage, St. Luis MO, *ASMR.*

Ward, A. S., M. N. Gooseff, and K. Singha (2010), Characterizing hyporheic transport processes - Interpretation of electrical geophysical data in coupled stream-hyporheic zone systems during solute tracer studies, *Adv. Water Resour., 33,*1320-1330.

White, P. A. (1994), Electrode arrays for measuring groundwater flow direction and velocity, *Geophysics 59*, 192–201.

Wiley, J. B., R. D. Evaldi, J. H. Eychaner, and D. B. Chambers, (2001), Reconnaissance of Stream Geomorphology, Low Streamflow, and Stream Temperature in the Mountaintop Coal-Mining Region, Southern West Virginia, 1999–2000, US Geological Survey: Charleston, WV, USA.

Wunsch, D. R., J. S. Dinger, and C. D. R. Graham (1999), Predicting ground-water movement in large mine spoil areas in the Appalachian Plateau, *Int. J. Coal Geol. 41*, 73–106.

Zégre, N. P., A. Maxwell, and S. Lamont (2013), Characterizing streamflow response of a mountaintop-mined watershed to changing land use, *Appl. Geogr., 39*, 5–15.

Zégre, N., A. J. Miller, A. Maxwell, and S. Lamont (2015), Multi-scale analysis of hydrology in a mountaintop mine impacted watershed. *J. Am. Water Resour. Assoc. (in press).*

Zipper, C. E., J. A. Burger, J. G. Skousen, P. N. Angel, C. D. Barton, V. Davis, and J. A. Franklin, (2011), Restoring forests and associated ecosystem services on Appalachian coal surface mines. *Environ. Manage. 47*, 751–765, doi:10.1007/s00267-011-9670-z.

Chapter 3 – Engineering Significance

Mountaintop removal mining (MTRM) or surface coal mining is the largest land use change in the Appalachian Coalfield Region. MRTM began with equipment advances and an increase in energy demand in the 1960's. While the practice is regulated by the EPA through the Water Quality Act and the Surface Mining Control and Reclamation Act, it is still not environmentally benign. Studies have shown that MTRM leads to water quality degradation in local headwater streams that impair local ecology for decades after the reclamation phase is complete. This water quality degradation is primarily due to the increase of total dissolved solids (TDS) caused when large volumes of crushed rock are subjected to accelerated weathering in both upland mine spoil piles and valley fills. It is through studying the flowpaths that water takes through these spoil structures that the pollution they cause may eventually be minimized. Previous studies have developed hydrologic models of MTRM impacted basins through input – output relationships and interpolation between point measurements, however flowpaths have never before been visualized directly.

The starting point for this thesis is the hydrologic, water quality, and biologic changes that occur within a MTRM watershed (Chapter 1) which serve as the motivation for the study presented in Chapter 2. The objectives of our study were to deploy ERI in a novel setting to track stormwater as it moves through a MTRM valley fill. In particular, we sought to develop an approach to successfully use ERI in this setting to 1) image the valley fill's geologic structure and compare that structure to a filled highwall slope and an unmined hillslope, and 2) image movement of subsurface stormflow within the fill including determining whether it is a uniform wetting front or preferential flow. We found that ERI is a suitable technology to use on valley fills because it is non-invasive, multi-dimensional, and removed the need for accurate input-output relationships interpolation between point measurements. We were able to visualize the fill's geologic structure and determined the upper portion of the fill more closely resembled soil while the lower portion is composed of large boulders and voids. By implementing artificial rainfall experiments on the fill we determined that the surface is compacted with minimal uniform infiltration, but that there were preferential flow paths that conducted water quickly and deeply at specific localities. These preferential flow paths were either horizontal, caused by conductive layers between compacted layers, or vertical, and extended deep into the fill.

The structure of the valley fill was also compared to two other landscapes, a slope adjacent to a filled highwall and a natural slope. It was noted that when compared to the filled highwall, a similar degree of variability was noted in the subsurface however data collection was more difficult at the highwall slope due to boulders at the surface. The natural slope showed a highly resistive layer which was the decomposing forest floor above relatively homogeneous bedrock with smooth transitions between materials. Showing that using ERI on each of the three landscapes produced an image that reflected the landscapes properties served as confirmation that ERI is able to decipher various subsurface structures in this setting.

This study may serve as a building block for future studies that may benefit the mining industry and surrounding communities. ERI may be used to compare flowpaths on various valley fill designs, such as the promising geomorphic valley fill design, and eventually aid in drawing

conclusions on how flowpaths impact water quality at the toe if the fill. Once these relationships are better understood, ERI could continue to be used to monitor flow paths in newly developed experimental low TDS valley fill designs. Our results have indicated that due to minimal matrix infiltration on the fill with preference toward preferential flow, much of effluent water TDS is likely generated in groundwater beneath the fill. Therefore, it may not be possible to retrofit existing valley fills, and may instead be worthwhile to conduct ERI studies on upland mine spoil piles. Both infiltrated stormwater and deep groundwater movement information would be useful in this instance. The development of either an impermeable membrane to prevent groundwater accumulation in the spoil or the exploitation of preferential flow to minimize the weathering potential could be valuable in increasing effluent stream water quality below. Improving headwater stream quality at the tops of these Appalachian watersheds will trickle through and result in improved water quality for the surrounding communities at the base of the watersheds.

Another useful application of ERI in an Appalachian coal mine setting would be to investigate the effect abandoned underground mines have on local hydrology. Many mine-related hydrologic studies cite abandoned underground mines as a confounding variable (Puente and Akins, 1989; McCormick et al., 2009; Petty et al., 2010); if the electrodes were spaced far enough apart (up 10 10 meter spacing), ERI could image these subsurface tunnel networks and provide insight to how they really impact local hydrology. Determining the frequency with which these abandoned underground tunnels evoke these hydrologic changes would be another important aspect of this work. We believe this could be an important area for future research.

Moving outside the realm of the Appalachian coal mining industry, ERI could be used in other mining applications. For example, with continued development ERI could replace the practice of coring as a subsurface exploration technique. ERI in non-invasive and does not require heavy machinery so it could be used to survey less accessible and more environmentally sensitive locations. ERI could also be used as a planning tool in pit mining as a survey could be done of the proposed pit location to confirm that subsurface lithology transitions as expected prior to excavation. With further development, ERI could be applied to a variety of resource harvesting industries.

The stated future uses of ERI in mined watersheds could help to ameliorate the water quality effects of Appalachian MTRM. With continued research and method improvements, harvesting coal for energy may become a preferred non-renewable energy option for the coming generation. However no amount of water quality improvement will make coal a renewable energy source. While we believe that this study as well as others that work toward making coal a cleaner energy source are paramount in protecting Appalachian ecology, we do not wish to undermine the need for renewable energy source development. The transition to clean coal will likely take decades and may contribute to climate change in the process. Eventually reliance on renewable energy sources, such as solar and wind, will be required due to dwindling non-renewable resources and the preservation of all natural systems in the meantime is preferred.

Appendix A- LTC Data Collection and Graphed Relationships

A-1: Introduction

Five Solinst Levelogger Juniors 3001 (Toronto, Canada) were installed in effluent streams below five valley fills and logged water level, temperature, and specific conductance (LTC) every 10 minutes from November 8th, 2013 to December 19th, 2014 (with one exception being at the fill presented in Chapter 2 at which data collection was disrupted on July 23rd, 2014 due to channel disruption and was not successfully continued thereafter). These LTCs served to aid in the selection of the fill used in the study by displaying the relationship between level and specific conductance (SC) throughout the year. They also are used in the creation of hysteresis curves for the relationship between level and SC for a future study.

A-2: LTC Calibration

The LTCs used at these sites did not calibrate via the Solinst provided calibration program because they had previously drifted too far from the correct values. Therefore, they were manually calibrated by creating linear conversion equations (e.g. Figure A-1). A three point calibration was completed using conductivity calibration solution standards provided by Solinst with specific conductivity values of 1,413 µS/cm, 5,000 µS/cm, and 12,880 µS/cm. Each probe was rinsed with deionized water when switching form one calibration solution to the next. The equation was then manually applied to conductivity readings during data processing. Note that each probe had a different calibration equation, so it is recommended to calibrate each LTC in this manner.

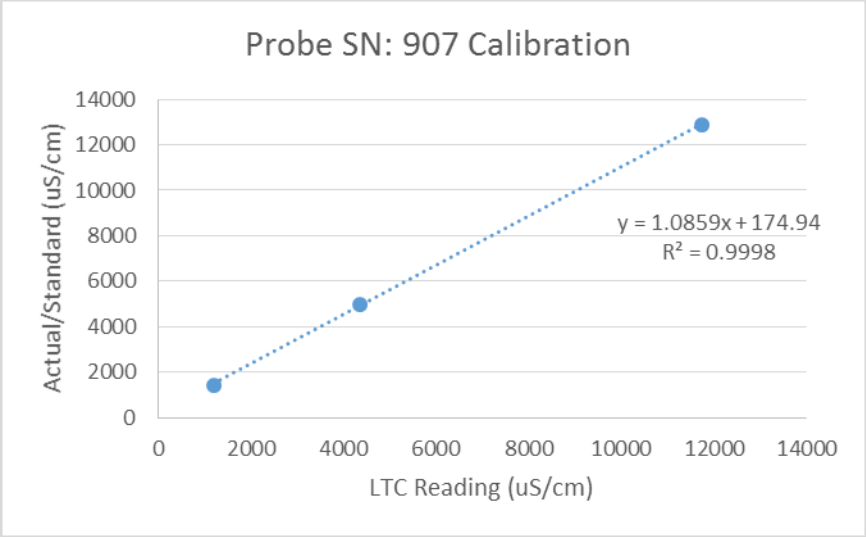

Figure A-1: Example of LTC Calibration Curve.

A-3: Site Selection

Site selection was an important component of LTC deployment. We aimed to install the LTC in a location that met the majority of the following conditions: near to point at which effluent stream emerges from fill toe, watershed above contains a minimal amount of non-mined land, all effluent stream channels are converged, the stream bed is composed of small enough rocks that the LTC may be securely installed. Often it was not possible to meet all of these criteria, however understanding these optimal conditions aided in site selection.

A-4: Installation and Maintenance

LTCs were installed into the streams by hammering a 1 m piece of rebar into the bed and attaching a short piece of PVC pipe with many large holes drilled into it and end capped (to serve as a protectant for the LTC) via band clamps. The LTC was then deployed and fastened to the inside of the PVC with zip ties for security.

Site visits occurred every four to eight weeks for LTC maintenance and data collection. Common activities in regards to maintenance were removing built up sediment from the LTC and its home, removing leaves that had blocked rapid LTC response to storm events, and bi-monthly acid washing of the LTCs with 1 M sulfuric acid (for 10 – 20 minutes) to remove biofilm. LTCs were never re-calibrated, however at each visit readings were also taken with a YSI Inc. conductivity probe to monitor for drift. These comparison values were monitored, but never included in final SC calculations because the variation between the YSI and the LTC varied significantly. A summary tale including YSI, raw LTC, calibrated LTC and the differences between the YSI and the LTC values (delta) can be seen in Table A-1. Due to these inconsistencies it is recommended to discontinue use of the Solinst Inc. LTCs in the future in preference of YSI, or another well reviewed company.

Table A-1. Comparison of YSI and LTC SC values. LTC values were never retrofitted with the YSI because the difference (delta) between collected values varied at each collection.

Date	**2/27/2014**	**4/1/2014**	**5/16/2014**	**7/23/2014**	**10/6/2014**	**11/15/2014**	**12/19/2014**
Site 1							
YSI	1305	1216	1275	1307	1421	1395	1406
Raw LTC	663	621	655	833	N/A	N/A	N/A
Delta	642	595	620	474			
Calib. LTC	951	911	944	1114	N/A	N/A	N/A
Delta	354	305	331	193			
Site 2							
YSI	1245	1275	1250	1393	1374	1321	1310
Raw LTC	584	826	834	844	804	327	794
Delta	661	449	416	549	570	994	516
Calib LTC	809	1072	1080	1091	1048	530	1037
Delta	436	203	170	302	326	791	273
Site 3*							
YSI	1650	1705	1824	1785	1885	1786	1784
LTC	1097	1132	1154	1364	1443	1331	1351
Delta	553	573	670	420	402	455	433
Site 4							
YSI	722.5	721	743	1127	868	1144	1024
Raw LTC	257	680	682	835	347	494	423
Delta	465.5	40	61	292	521	650	601
Calib. LTC	434	898	899	1067	533	693	616
Delta	288.5	-177	-156	60	335	451	408
Site 5							

YSI	1678	1667	1636	1558	N/A	1657	1710
Raw LTC	1385	1394	1367	1062	N/A	841	932
Delta	293	273	269	496		816	778
Calib. LTC	1885	1894	1869	1587	N/A	1382	1467
Delta	-198	-217	-233	-29		275	243

* Site 3 was successfully calibrated with the Solinst provided software before being launched and was not manually calibrated or adjusted throughout.

A-5: Data Processing

LTC data processing is not straightforward, so an example of spread sheet layout will be helpful to the next person to use these instruments (Table A-2).

Table A-2. Data Processing for LTC output file. Row 1 is the title of the data in the column, row 2 is how that column was calculated (if it was calculated), and rows 3-6 are example data from a LTC file used in this study.

Date	Time	LEVEL (m)	Level Adj (m)	Hobo (Kpa)	Hobo Adj (m) (/specific weight)	Water Level (cm)	TEMP (C)	SC (us/cm)	Calibrated EC
			Level + 9.5		Hobo/9.8	(LevelAdj - Hobo)*100			=EC*m+b
9/4/2014	15:30:00	0.148	9.648	94.099	9.6019	4.606	23.45	1056.2	1308.5
9/4/2014	15:40:00	0.147	9.647	94.084	9.6004	4.659	23.33	1056.2	1308.5
9/4/2014	15:50:00	0.154	9.654	94.103	9.6023	5.165	23.2	1053.5	1305.5

A-6: Complete LTC Graphs Not Included in Journal Article

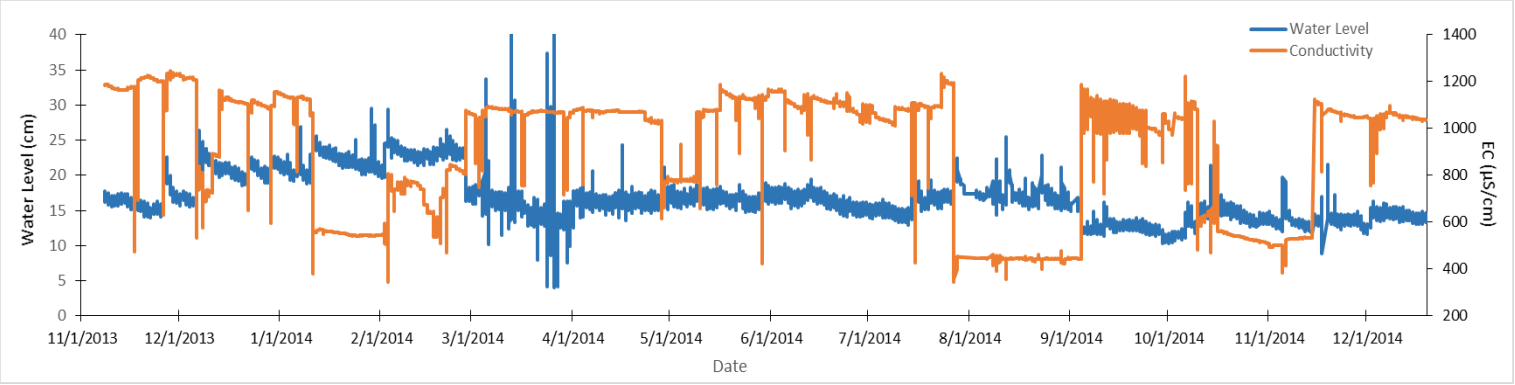

Figure A-2. LTC Data, November 8th, 2013 to December 19th, 2014 for Site 2.

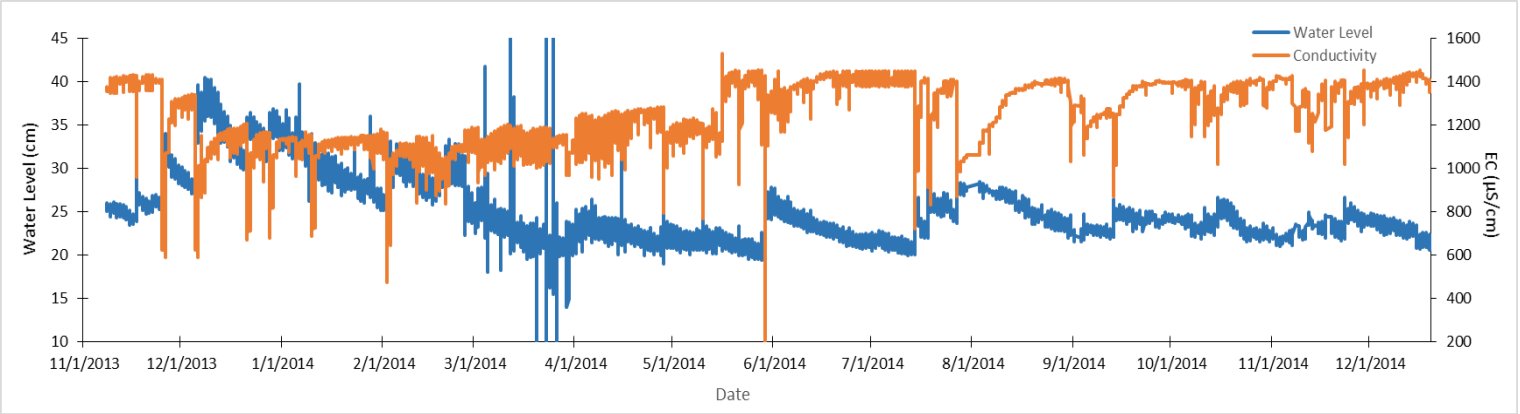

Figure A-3. LTC Data, November 8th, 2013 to December 19th, 2014 for Site 3.

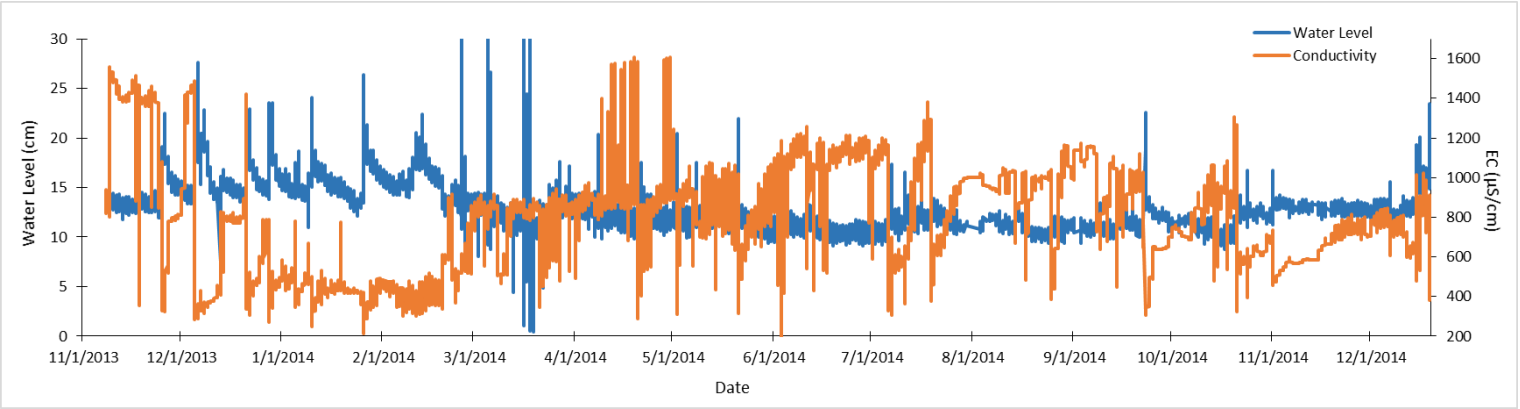

Figure A-4. LTC Data, November 8th, 2013 to December 19th, 2014 for Site 4.

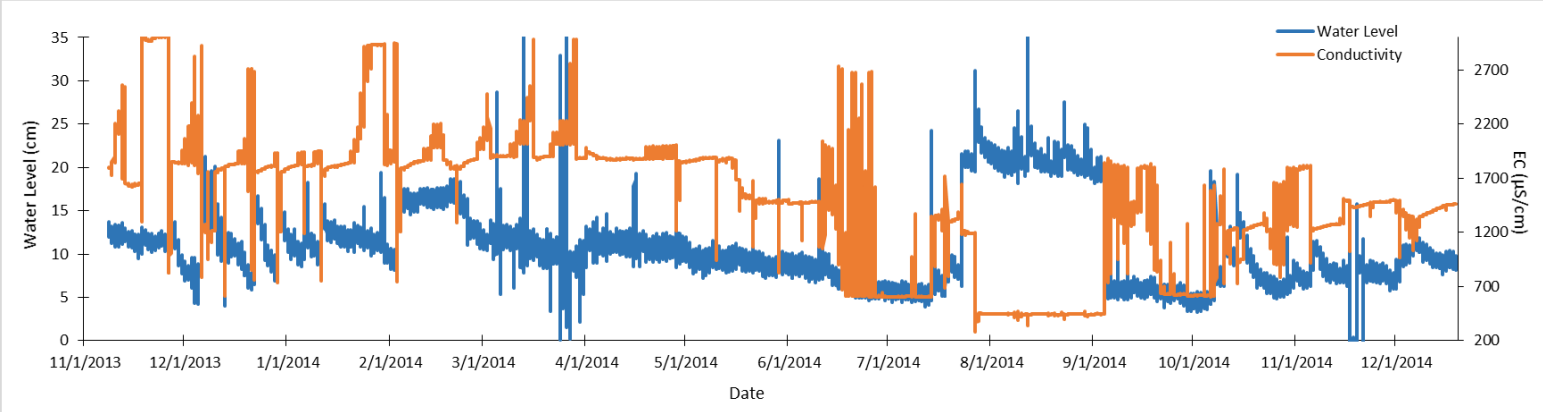

Figure A-5. LTC Data, November 8th, 2013 to December 19th, 2014 for Site 5.

A-7: Example Hysteresis Plots (Incomplete)

Below is a small sample of hysteresis plots that will likely be used in a future study on the relationship between water level and SC in valley fill effluent streams. Each plot represents a single storm at a single fill. For an idea of the type of study this will be used in, see Murphy et al., (2014) cited at the bottom of this section.

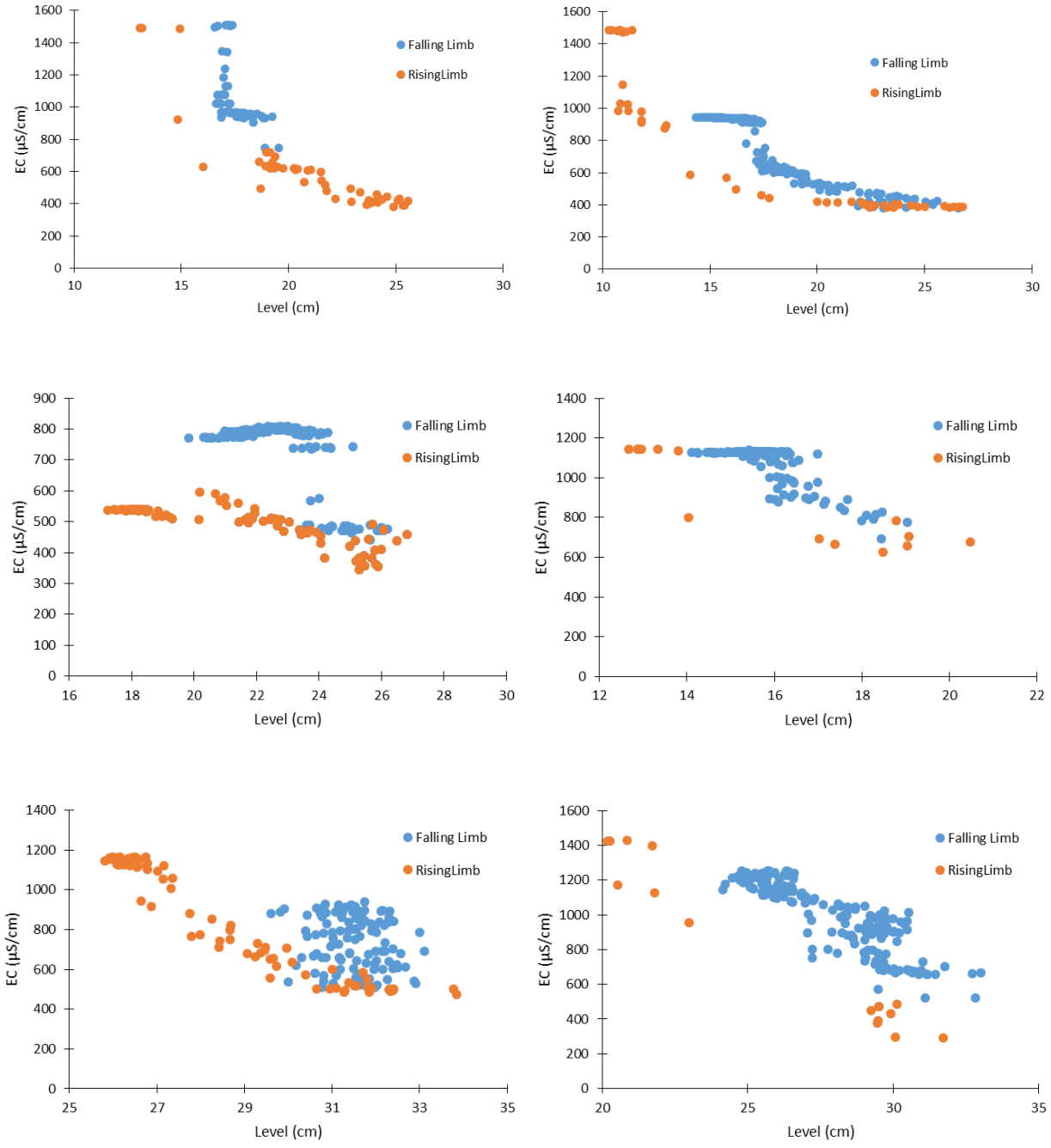

Figure A-6: Example Hysteresis Plots for all sites. Panel A: Site 1, January 11, 2014. Panel B: Site 1, February 3, 2014. Panel C: Site 2, February 3, 2014. Panel D: Site 2, May 29. 2014. Panel E: Site 3, February 3, 2014. Panel F: Site 3, May 29, 2014.

Murphy, J. C., G. M. Hornberger, and R. G. Liddle (2014), Concentration-discharge relationships in the coal mined region of the New River basin and Indian-Fork sub-basin, Tennessee, USA, *Hydrol. Process.*, *28*, 718-728, doi:10.1002/hyp.9603.

Appendix B - Artificial Rainfall Experiment and ERI Additional Information

B-1: Complete Table of ERI Surveys Taken.

A complete list of surveys done in this study is presented below. The journal article does not contain all of the surveys for multiple reasons. There would have been too many figures in the article, such that adequate attention could not be paid to each of them. Some of the survey findings were repetitive but at a larger scale, with precipitation lasting a shorter length of time, or the results being less clear; in which more detailed surveys were preferred. Finally, there was one survey excluded because it had a larger rainfall plot and would not be directly compared to the other. We believe none of the excluded surveys to present contradictory information to what is included in the journal article.

Table B-1. Complete Table of ERI Survey Series Properties. Presented here are the ERI survey series by electrode spacing, transect length, rainfall time between surveys, and dry time before rainfall onset.

Survey Series	Date	Electrode Spacing	Transect Length	Rainfall Duration	Time Interval Between Surveys	Pre-rainfall Dry Time *
Vertical (dry)	7/31/2014	5 m	300 m	N/A	N/A	4 days
Vertical (wet)	5/23/2014	5 m	300 m	N/A	N/A	2 hours
Horizontal (dry)	5/22/2014	3 m	190 m	N/A	N/A	4 days *
Artificial Rain 2.5m (RN1X)	6/30/2014	2.5 m	160 m	2:15 hr	1:00 hr	5 days
Artificial Rain 2.5 m (RN2X)**	7/10/2014	2.5 m	160 m	2:15 hr	0:45 hr	1 day
Artificial Rain 1.5m (RN4X)	7/17/2014	1.5 m	96 m	5 hr	1:15 hr	2 days
Artificial Rain 1.5m (RN6X)	8/1/2014	1.5	96 m	3 hr	1:00 hr	1 day
Artificial Rain 1.0m (RN3X)	7/11/2014	1.0 m	64 m	2:15 hr	0:45 hr	16 hours
Artificial Rain 0.5m (RN5X)	7/31/2014	0.5 m	32 m	2:15 hr	0:45 hr	4 days
Highwall (dry)	8/13/2014	2.0 m	128 m	N/A	N/A	2 days *
Natural Slope (dry)	11/15/2014	2.0 m	128 m	N/A	N/A	7 days *

* For surveys taken on dates without a weather station on site, rainfall data was taken from the NOAA weather station, Wise VA (#44-9215).

** The X in RN4X etc. signifies that there are multiple surveys in the experiment titled RN4.

B-2: Tomograms Not Presented in Journal Article

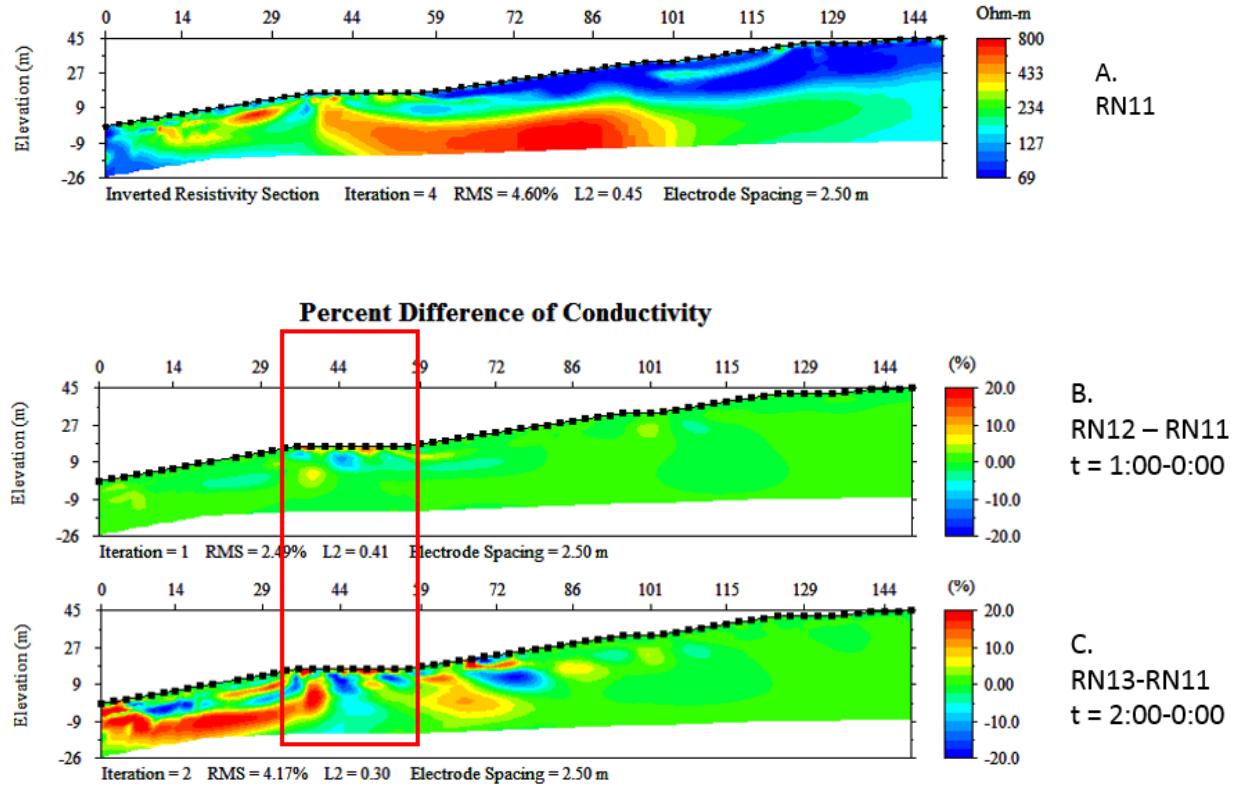

Figure B-1. Individual Resistivity and Time-Lapse Tomograms of RN1X Artificial Rainfall Experiment with 2.5 m spacing. Panel A is the dry individual resistivity inversion tomogram while panels B and C are time-lapse tomograms during the artificial rainfall experiment.

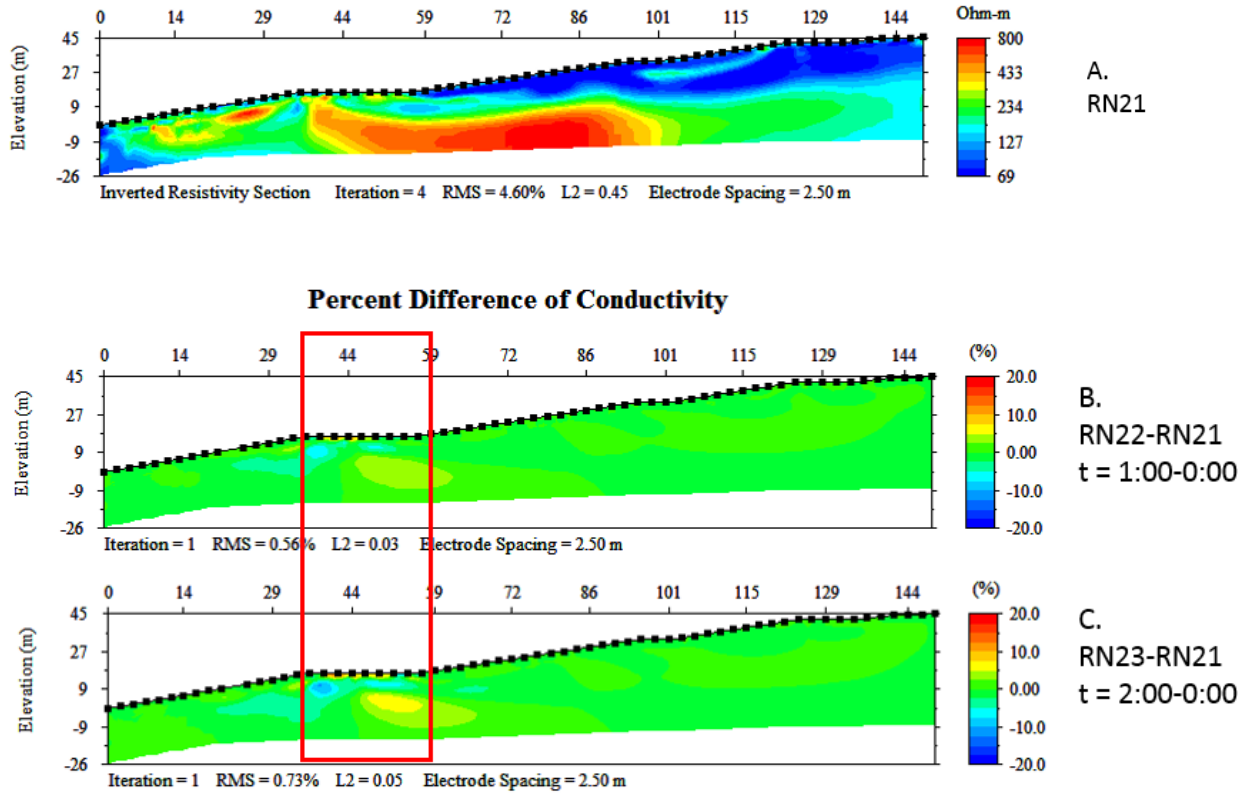

Figure B-2. Individual Resistivity and Time-Lapse Tomograms of RN2X Artificial Rainfall Experiment with 2.5 m spacing. Panel A is the dry individual resistivity inversion tomogram while panels B and C are time-lapse tomograms during the artificial rainfall experiment.

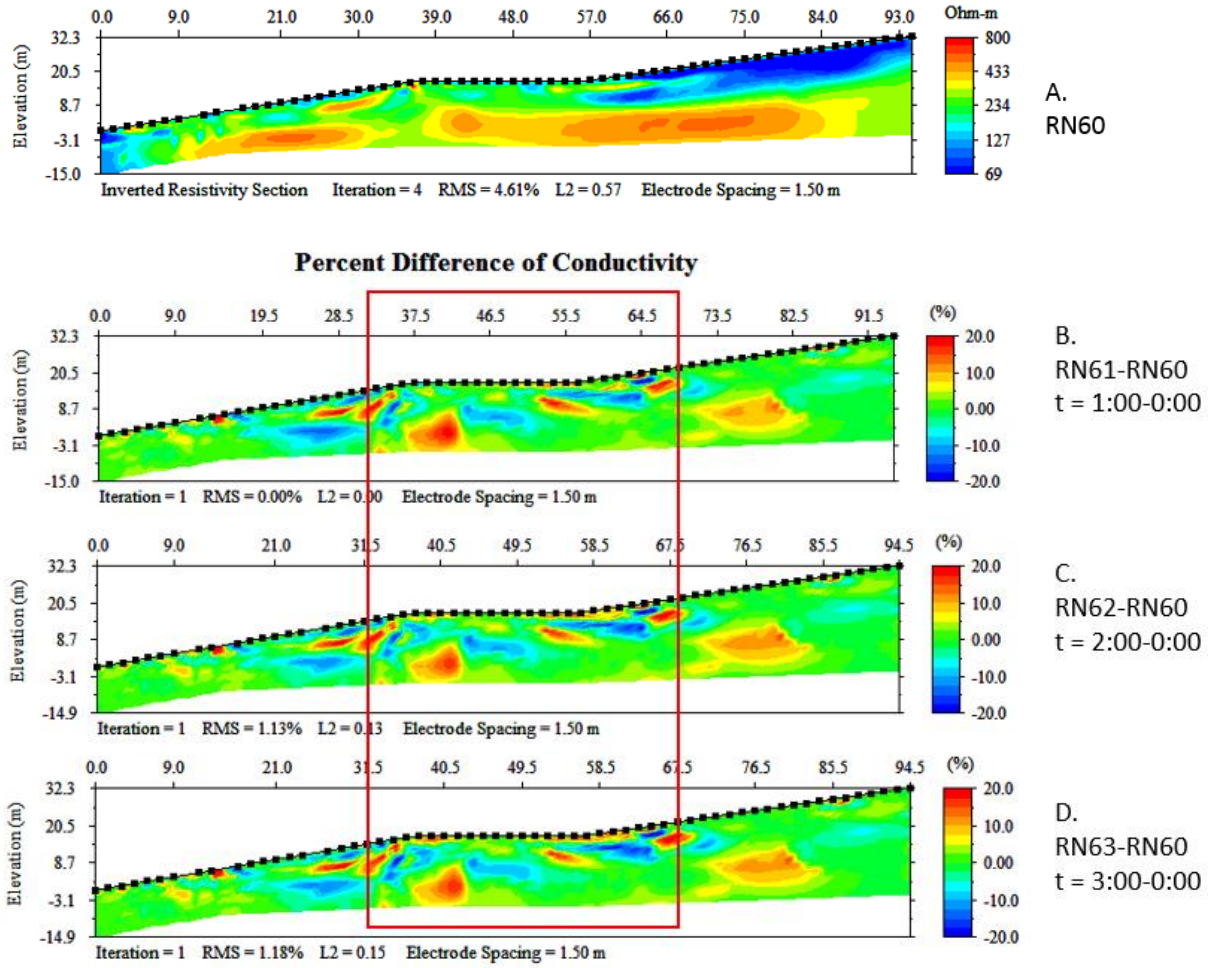

Figure B-3. Individual Resistivity and Time-Lapse Tomograms of RN6X Artificial Rainfall Experiment with 1.5 m spacing. Panel A is the dry individual resistivity inversion tomogram while panels B and C are time-lapse tomograms during the artificial rainfall experiment. Note that this one has a larger rainfall plot than the rest, and thus changes are seen further upslope than the others.

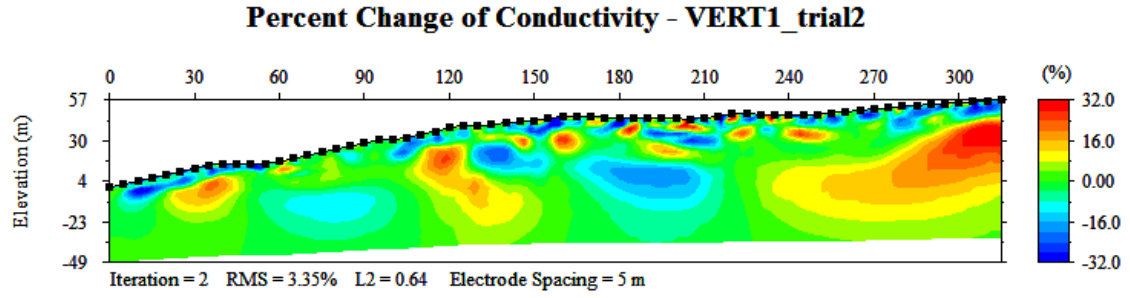

Figure B-4. Time-Lapse Tomogram of VERT, Natural Rainfall with 5.0 m spacing. This was done with the control in dry conditions and the monitor survey in wet conditions, 8 hours after a natural rainfall event.

Individual Resistivity Tomograms

Individual resistivity inversion tomograms (i.e. not time-lapse) can also reveal movement of water through the fill (although less definitively). This increase in water content results in a decrease in resistivity (less yellow-orange, more green-blue) with time (Figure 2-10). RN41 is the analogous survey done in dry conditions. In RN42 at time 1:15 the area beneath the rainfall plot (35-40 m) appears to become less resistive, even at a depth of -15 m (Figure 2-10b). By time 2:30 (Figure 2-10c), the decrease in resistivity has continued and extended slightly to the left. Finally, RN41 also serves as a confirmation of the presence of a resistive (orange) layer above a compacted (blue) shelf between meters 18 and 35 (black box, Figure 2-10a). The resistive layer is more transmissive and becomes inundated and disappears after the onset of the rainfall (black box, Figure 2-10b). This is also captured by the increasing conductivity along the flow path in the time-lapse tomogram (black box, Figure 2-7d).

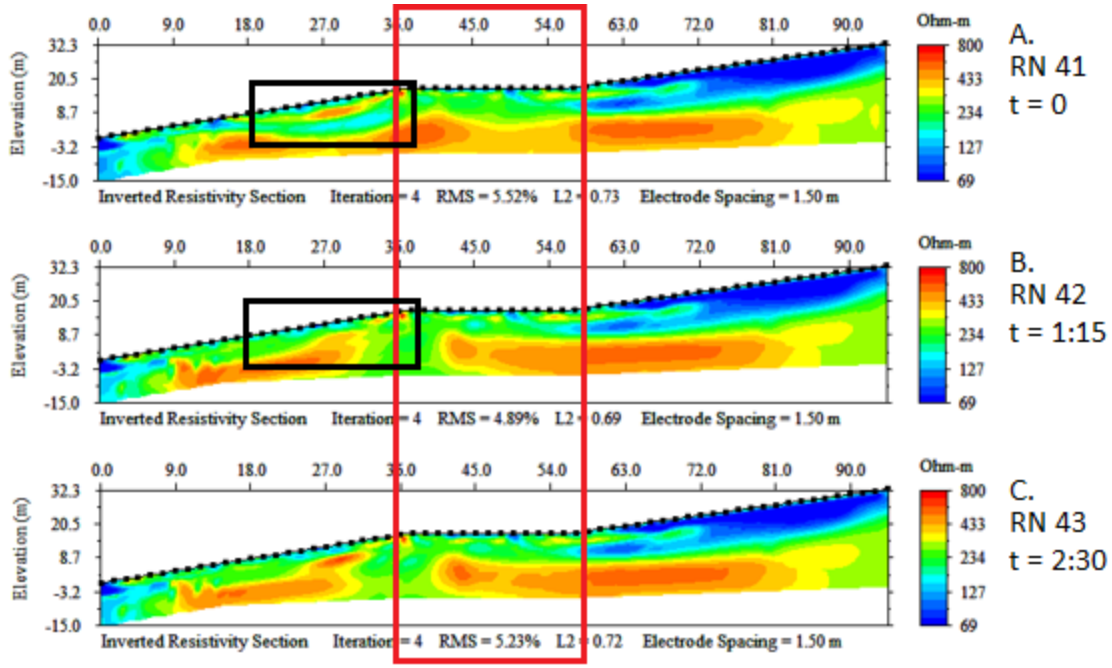

Figure B-5. Tomograms of artificial rainfall experiment with 1.5 meter spacing. Individual resistivity tomograms showing electrical resistivity (Ohm-m) where areas of greater electrical resistivity are red. These show that water infiltration can be also seen in time-lapse tomograms. The corresponding time-lapse tomograms are shown in Figure 2-7. July 17, 2014. Red box indicates location of rainfall plot. Black box shows preferential flow path development.

B-3: Conductivity Values of Artificial Rainfall Experiments

Table B-2. Specific Conductance and Depth Values of Artificial Rainfall Experiments. This table includes specific conductance values of the artificial rain for each of the experiments. Values were measured with a YSI Inc. conductivity probe at the pond inlet. Note that the times here are presented as both time of day and time since precipitation for the greatest degree of accuracy.

Survey Series	Date	Time (of day)	SC (µS/cm)	Time (since precip. onset)	Avg. Precip. Depth (cm)
RN1X	6/30/2014	4:00	1261		
		4:30	1248		
		5:00	1225	1:00	1.7
		5:30	1195		
		6:00	1170	2:00	3.39
		6:30	1142		
RN2X	7/72014	5:40	1300		
		6:40	1283	1:00	0.76
		7:40	1285	2:00	3.89
RN3X	7/8/2014	10:55	1321		
		12:20	1308	0:45	1.35
		1:05	1305	1:30	2.46
		1:50	1306	2:15	6.14
		2:35	1297		
RN4X	7/17/2014	9:40	864		
		10:55	867	1:15	1.27
		12:10	868	2:30	3.09
		1:25	864	3:45	4.87
		2:40	870	5:00	6.65
RN5X	7/31/2014	9:00	1125		
		9:45	1138	0:45	1.40
		10:30	1146	1:30	3:13
		11:15	1152	2:15	4.49
RN6X	8/1/2014	9:10	1206		
		10:10	1209	1:00	0.93
		11:10	1210	2:00	1.61
		12:10	1212	3:00	2.41